UNIVERSITY OF CALIFORNIA, SAN DIEGO

Fluorescence-based Investigations of the Dynamics and Properties of Cell Penetrating Peptide Cellular Uptake Mechanisms

A dissertation submitted in partial satisfaction of the requirements for the degree

Doctor of Philosophy

in

Chemistry

by

Sujata R. Emani

Committee in charge:

Professor Roger Y. Tsien, Chair
Professor Edward A. Dennis
Professor Daniel J. Donoghue
Professor Mark A. Ellisman
Professor Akif Tezcan

2012

The Dissertation of Sujata R. Emani is approved, and it is acceptable in quality and form for publication on microfilm and electronically:

_____

_____

_____

_____

_____

Chair

University of California, San Diego

2012

Dedication

For my teachers, mentors, and My Highest Guru.

Epigraph

It doesn't matter
if you fall down
as long as
you pick up
something
from the floor
while you get up.

Efraim Racker

Table of Contents

List of Figures

List of Tables

Acknowledgements

There are many people who have helped me to arrive at this accomplishment. Thank you to the entire Tsien Lab who taught me, laughed with me, and guided me when frustration got the best of me. Special thanks to Nathan Shaner, S. Andrew Hires, Stephen Adams, Paul Steinbach, Qing Xiong, Jin Yang, Richard Ting, John Lin, Varda Levram-Ellisman, and Joan Kanter for your camaraderie and vibrant discussions. I greatly appreciate my committee members Profs. Ed Dennis, Dan Donoghue, Mark Ellisman, and Akif Tezcan for their honest feedback, critical evaluation, and guidance throughout my graduate career. I have the greatest admiration and respect for Prof. Roger Y. Tsien for continually inspiring me, allowing me to learn at my own pace, and posing challenging questions to make me a better scientist through this process.

I was in love with nature, science, and math long before I was in research and my teachers are to thank for inspiring my pursuits. Most special thanks to Mindy Bedrossian, my teacher and good friend, for showing me how easy it is to love Chemistry and who lit the fire in my belly to relentlessly ask, "Why?"

I am forever indebted to Professor Terry Rosenberry and Bernadette Cusack, who showed me that perseverance and dedication to a subject could set you on a fulfilling journey for a lifetime. To my wonderful friends and colleagues who let me grow and learn to be a scientist: Mike Patrick, Lauren Ernst, Greg Fisher, Brigitte Schmidt, Sue Andreko, Byron Ballou, Jason Smith, and Alan Waggoner.

To my loving, compassionate, patient, and enthusiastic friends who gave me strength when I needed it most: Malisha Pattanaik, Priyal Sheth, Sanket Pingle, Nikki

Justis Truitt, Ed Truitt, Shivani Singh, Gloriana Gallegos, C. Nicholas Saenz, Gizelle Sherwood, Travis Palmer, Jim Buccini, Heather and J Keirn-Swanson, Matt Neifer, Nishil Dalsania, James Finlay, Robert Butler, Tricia Tanguy, and Jon Ipsaro.

Thanks to my siblings, Nirmala, who always reminds me that no matter what, everything will always be OK, Taruna, who reminds me to just have fun, and Ranga, who makes me laugh to no end. To my fantastic step-mom, dad, Babai, Pinni, and Harsha, whose love and advice have been nourishing to my soul at just the right moments, thanks for encouraging me, supporting me, and helping me with coding and math problems at all hours of the night and day; I hope you know that I live to make you proud. To my humble, loving, and effortlessly impressive Grandmother, Indurani, thank you for giving me solace and comfort and inspiring my life.

I could never have accomplished anything if it was not for my mom, Vijaya L. Emani. Her love, blessings, support, and guidance in-person and in-spirit have provided me the energy and determination to persevere through all challenges. Although, she is not here to witness the completion of my doctorate with her eyes, I know that she has been with me everyday. She provides me with a guiding light whenever I am lost. Her love and friendship gave me all the lessons I needed in life. In light of those imparted lessons, this achievement is *just three extra letters*.

Chapter two and three are currently being prepared for submission for publication. The dissertation author was a primary author. Co-authors include Dr. Stephen R. Adams, and Dr. Roger Y. Tsien. Thanks is extended to Paul Steinbach for training and assistance with epifluorescence imaging, confocal imaging, and microcuvette calibrations and calculations. Additional thanks must be extended to Dr. Kaoru Saijo for reagents for pH

sensor calibrations. Chapter four is currently being prepared for submission for publication. The dissertation author was a primary author. Co-authors include Dr. Andrew Dix, Dr. Yitzhak Tor, and Dr. Roger Y. Tsien.

Curriculum Vitae

EDUCATION

Ph.D. in Chemistry, 2012
Universiy of California, San Diego, La Jolla, California

M.S. in Chemistry, 2005
Carnegie Mellon University, Pittsburgh, Pennsylvania

B.S. in Chemistry, 2005
Carnegie Mellon University, Pittsburgh, Pennsylvania

RESEARCH EXPERIENCE

Doctoral Research
University of California, San Diego, September 2005 – August 2011
Advisor: Roger Y. Tsien

- Determined the efficiency of polyarginine cell penetrating peptide to deliver a fluorescent payload to the cytosol of mammalian cells measured by FRET and Fluorescence microscopy
- Uncovered previously unreported cooperativity in the cytosolic delivery rate of the payload by polyarginine peptides.
- Provided rate and biochemical details of the endocytic pathway of polyarginine CPP uptake

Master's Research
Carnegie Mellon University, MBIC, June 2004 – August 2005

- Enabled the use of commercial dyes and newly synthesized dyes for detection of microbes in biofilms by a prototype Mars rover
- PI: Prof. Alan S. Waggoner, Ph.D.

Independent Student Researcher
NASA-JSC Reduced Gravity Flight Program, December 2003 – August 2004

- Executed a unique study aboard the KC-135 Reduced Gravity Research Aircraft on the affect of micro-gravity on primary human lymphocytes with funding from HHMI and NASA JSC Reduced Gravity Flight Opportunities Program
- Advisor: Prof. Adam Linstedt, Ph.D.

Undergraduate Student Researcher
Carnegie Mellon University, MBIC, October 2003 – June 2004

- Synthesis of fluorescent voltage sensor dyes
- Applied extensive organic synthesis methods and techniques

- PI: Prof. Alan S. Waggoner, Ph.D.

Student Researcher
The Mayo Clinic, Jacksonville, June 2003 – August 2003
- Studied the biochemical kinetics of carbamoylation in Acetylcholinesterase
- PI: Prof. Terry L. Rosenberry, Ph.D.

TEACHING EXPERIENCE

University of California, San Diego, Biobridge
Mentor, June 2006 – June 2009
- Introduced new tools for high school teachers to utilize in the science curriculum and mentored high school students in underserved communities in San Diego.
- Bridged local high school teachers, students, and academic researchers to create a new network for education resources.

University of California, San Diego, Extension
Teacher, Academic Connections Summer Pre-College Program, July 2007
- Created and taught a lab-based biotechnology curriculum for advanced high school students in cell biology

University of California, San Diego
Teaching Assistant, Department of Chemistry and Biochemistry, Jan. 2006 - April 2007
Organic Chemistry Lab, Chemistry of Biology, Physical Chemistry

PUBLICATIONS AND PRESENTATIONS

Emani, S.R., Adams, S.R., Tsien, R.Y., FRET-based quantitation and characterization of the D-Arginine9 CPP cellular uptake pathway. Manuscript in preparation.

Dix, A., **Emani, S.R.**, Esko, J., Tsien, R.Y., Tor, Y., Quantifying Cytosolic Delivery of Guanidinium-based Molecular Transporters. Manuscript in preparation.

Emani, S.R., Adams, S.R., Tsien, R.Y., FRET-based investigations into poly-arginine CPP cellular uptake mechanism. American Chemical Society National Meeting Fall 2010, Boston, MA (abstract #243).

Weinstein, S., D. Pane, L. A. Ernst, K. Warren-Rhodes, J. M. Dohm, A. N. Hock, J. L. Piatek, **S. Emani**, F. Lanni, M. Wagner, G. W. Fisher, E. Minkley, L. E. Dansey, T. Smith, E. A. Grin, K. Stubbs, G. Thomas, C. S. Cockell, L. Marinangeli, G. G. Ori, S. Heys, J. P. Teza, J. E. Moersch, P. Coppin, G. C. Diaz, D. S. Wettergreen, N. A. Cabrol, and A. S. Waggoner (2008), Application of pulsed-excitation fluorescence imager for

daylight detection of sparse life in tests in the Atacama Desert, *J. Geophys. Res.*, 113, G01S90, doi:10.1029/2006JG000319.

Warren-Rhodes, K., S. Weinstein, J. L. Piatek, J. Dohm, A. Hock, E. Minkley, D. Pane, L. A. Ernst, G. Fisher, **S. Emani**, A. S. Waggoner, N. A. Cabrol, D. S. Wettergreen, E. Grin, P. Coppin, C. Diaz, J. Moersch, G. G. Oril, T. Smith, K. Stubbs, G. Thomas, M. Wagner, M. Wyatt, and L. N. Boyle (2007), Robotic ecological mapping: Habitats and the search for life in the Atacama Desert, *J. Geophys. Res.*, 112, G04S06, doi:10.1029/2006JG000301.

Warren-Rhodes, K., S. Weinstein, J. Dohm, J. Piatek, E. Minkley, A. Hock, C. Cockell, D. Pane, L. A. Ernst, G. Fisher, **S. Emani**, A. S. Waggoner, N. A. Cabrol, D. S. Wettergreen, D. Apostolopoulos, P. Coppin, E. Grin, C. Diaz, J. Moersch, G. G. Oril, T. Smith, K. Stubbs, G. Thomas, M. Wagner, and M. Wyatt (2007), Searching for microbial life remotely: Satellite-to-rover habitat mapping in the Atacama Desert, Chile, *J. Geophys. Res.*, 112, G04S05, doi:10.1029/2006JG000283.

Johnson JL, Thomas JL, **Emani S**, Cusack B, Rosenberry TL. Measuring carbamoylation and decarbamoylation rate constants by continuous assay of AChE. *Chemico-Biological Interactions* (2005) Dec. 15:384-385, doi:10.1016/j.cbi.2005.10.066

Rosenberry TL, Johnson JL, Cusack B, Thomas JL, **Emani S**, Venkatasubban KS. Interactions between the peripheral site and the acylation site in acetylcholinesterase. *Chemico-Biological Interactions* (2005) Dec. 15:181-189, doi:10.1016/j.cbi.2005.10.027

Warrren-Rhodes, K., S. Weinstein, D. Pane, C. Cockell, J. M. Dohm, J. Piatek, L. A. Ernst, E. Minkley, G. Fisher, **S. Emani**, D. S. Wettergreen, M. Wagner, N. A. Cabrol, A. S. Waggoner 2005. Mars analog habitat survey and the search for microbial life remotely with an autonomous astrobiology rover. UV. *NAI 2005 Biennial Meeting*, University of Colorado, Boulder, Center for Astrobiology, (abstract #861).

AWARDS AND HONORS

Edward A. Bouchet Graduate Honor Society - 2010
UCSD Graduate Students Association, Outstanding Graduate Student 2008
Michael G. Rosenfeld Medical Training Grant Recipient 2006 - 2011
National Dean's List 2005
Dean's List Spring 2003, Spring 2004, Spring 2005
Carnegie Mellon Women's Alumni Section 2004 Scholarship
American Society of Engineers of Indian Origin Scholarship 2004
Sigma Xi Poster Competition Finalist 2004

ABSTRACT OF THE DISSERTATION

Fluorescence-based Investigations of the Dynamics and Properties of Cell Penetrating Peptide Cellular Uptake Mechanisms

by

Sujata R. Emani

Doctor of Philosophy in Chemistry

University of California, San Diego, 2012

Professor Roger Y. Tsien, Chair

Therapeutic drug delivery to diseased tissues and organs specifically and without toxicity to the body is a huge challenge in the field of medicine and pharmaceutical chemistry. Researchers are investigating a variety of methods to overcome the various membranous biological barriers to gain entry into a diseased cell. Cell penetrating peptides (CPPs) received a lot of attention in the last two decades as a tool that could solve the drug delivery problem. Although there has been broad and continued interest in CPPs for their ability to innocuously and efficiently deliver therapeutics into individual

cells, there is still much to understand about the cell entry mechanism and methods to evaluate the efficiency of entry have been lacking. To provide a thorough analysis of the CPP delivery efficiency, clarify the details of the mechanism, and characterize the pathway of cell entry, here we present an analysis of one CPP, D-arginine$_9$ (r_9). Using unique fluorescence based and FRET assays we show that r_9 is able to enter the cytosol and delivery a cargo at a rate and concentration that indicates that it can be potentially very useful for drug delivery. Additionally, we have discovered that intramolecular dimers of r_9 molecules can escape into the cytosol at rates 4-6x fold better than monomers. Furthermore, we discovered that endocytic vesicles containing the r_9 molecules are rapidly acidified within 28 minutes and furthermore there is indication that acidification prevents the release of these peptides into the cytosol. To provide reference to a non-peptide drug delivery technology, we compare the rate of r_9 cytosolic entry to a non-peptide guanidinium molecular transporter, Guanidinylated Neomycin using the same FRET assay. Finally, using common biochemical inhibitors of various aspects of endocytosis, we provide some evidence of the promiscuity of the endocytic routes by which r_9 may be gaining entry to the cytosol. It is our hope that these data provide some insight for future directions of the drug delivery field of study.

Chapter One

Introduction

Delivery efficiency and efficacy is a major challenge in the usage of peptide, protein, and nucleic acid based therapy for human diseases.[1] Another challenge to drug therapy is localized targeting to the site of action of a disease inside the infected cell.[1] These major barriers keep many drugs from getting past the discovery stage of pharmaceutical research and development, thus preventing them from ever reaching therapeutic and clinical trials necessary to treat patients with the disease. For this reason, the medical and pharmaceutical industry actively focus on improving therapeutic drug delivery.

Development of drug delivery methods is constrained by physiological requirements: immunogenicity, size, and usage in clinical practice. Formulation of drugs and drug coatings in the body can result in an attack by the immune system or the size of the entire macromolecule containing a therapeutic may be large enough to accumulate in macrophage phagocytic system cells in the kidneys and liver before they can reach the diseased region. Pharmaceutical companies have been in search for delivery methods that optimize these three requirements and can provide a significant improvement of the effectiveness while also reducing the cost of preparation of these molecules.

Cell penetrating peptides: A new class of delivery molecules

Over the past two decades nanoparticles and lipophilic vesicles have been the main focus, but are often large in size and even when taken into cells may become sequestered in endocytic vesicles and subcellular organelles.[2] An unusual class of peptides had been noted for the ability to fully overcome the cellular membrane and gain entry into the cytoplasm and nucleus of cells, seemingly not sequestered in subcellular

compartments as nanoparticles are. This class of peptides had been first identified from natural sequences in HIV-1 trans-activator of transcription protein (TAT peptide) and in *Drosophila* homeobox domain protein antennapedia (Penetratin).[3,4,5,6,7] These short peptides, designated as cell penetrating peptides (CPPs, Table 1.1), were implicated to mediate active cellular uptake and release of their larger protein complexes into cellular cytoplasm and nucleus.[8] In the case of Penetratin, it was implicated in allowing the inter-cellular uptake of the full-length antennapedia to bind and promote transcription of DNA in adjacent neuronal cells.[5] Since the original discovery of TAT and Penetratin, other peptides were discovered, developed, and are continually being improved.[9,10,11]

CPP categories

CPPs can be divided into two main categories based on their chemical properties: amphipathic peptides and cationic peptides. Amphipathic peptides correspond to peptides composed of both neutral and hydrophilic amino-acids and cationic peptides contain mainly positively charged amino-acids (Table 1.1). CPPs in both categories are widely investigated to delineate the pathway of cellular uptake, efficiency, and efficacy of delivery of therapeutic compounds and imaging molecules. Examples of both amphipathic peptides and cationic peptides are shown to deliver covalently bound small molecule cargo as well as siRNA through complex formation.[12,13,13] These peptides are recognized for their potential to deliver bio-active molecules to the inside of cells, but the field continues to face many challenges to improve the efficiency and understand how to make the most useful delivery vehicle that can target the correct region of the cell. While there appeared to be many different routes and mechanisms of uptake, the consensus is that the pathways are all energy-dependent. To understand the range of molecules that

can be delivered by CPPs investigators use a wide range of appended cargoes that diverge from Lipinski's rule to test the utility of CPPs: small molecules[13], nucleic acids[15], proteins[7,16], and quantum dots[17]. Delivery effectiveness, kinetics, and the endocytic pathway of the mechanism were also cargo-dependent and not simply determined by the CPP character.

CPP Mechanism Studies

Variability in the pathway of uptake as well as the delivery kinetics ignited an interest in the localization and quantification of delivery of CPP into cells and tissues. To achieve this CPP cytosolic entry was monitored by methods and tools used in both biological and chemical analysis.[18] Tools and methods from biology offer answers regarding effectiveness of CPPs to deliver biologically active molecules to the cytoplasm by escaping the endosome and interfering with protein expression.[7,19] Methods and tools from chemistry encompass analytical measurements to quantify and differentiate CPPs within specific compartments of the cell using chemical modification.

Biological methods to assay CPP effectiveness have monitored responses such as: the induction of apoptosis or non-proliferation, splice correction by interfering oligonucleotide, Cre-recombinase integration of a functional gene, fluorescence activated cell sorting monitoring internalized CPP and cargo, electron microscopy, and live cell microscopy. Dowdy and colleagues reported several full-length proteins conjugated to TAT that could be endocytosed into cells and produce a cellular response thus indicating that at least some of the peptide and cargo had been released into the cytosol of cells and reached the nucleus and DNA.[19] However, single cell studies indicate partial delivery of these peptides and their cargo to the intracellular compartment of mammalian cells, while

others reported the extensive endosomal trapping of the peptide and cargo and sequestration of the therapeutic cargo from the target site.[20] Biological methods are beneficial for understanding the CPP uptake in a live cell or can monitor the actions of the cell visually, however these methods often observe these reactions after a delay or, as in microscopy, are highly dependent on resolution limits of light.

Chemical methods aim to provide an exact number or a relative number for the delivery of the CPP molecules. HPLC, quantitative spectrofluorimetry, and mass spectrometry all provided more analytical and quantitative measurement of the CPP and its cargo once removed from the biological system. Bienart's group used degrees of chemical modification to distinguish membrane bound, partially internalized, and cytosolic peptide by injecting cell lysates through an HPLC.[21] Burlina's group pioneered a quantitative measurement of internalized CPPs using mass spectrometry.[22] Chemical methods have the advantage of being able to quantify exact amount of peptides that are internalized by utilizing highly sensitive analytical instrumentation. Similar to biological methods, chemical methods also require a delay between the cell experiment and the quantitative analysis and often require extensive post-experiment manipulation, but provide the opportunity for a more exact measurement of the compartmentalized CPP.

Although many methodologies have been developed, the CPP uptake process continues to be an active field of investigation to uncover the time-resolved finer details of the mechanism. The work presented in this dissertation will address finer details of the kinetics and dynamics in real-time of one particular CPP, polyarginine (D-arginine$_9$, r$_9$, Table 1.1).

Chapter two addresses the uptake process and the delivery kinetics of the uptake process of polyarginine (r_9) peptides. Using FRET and live microscopy the delivery kinetics for r_9 was elucidated. By applying a mathematical model of cooperativity for the delivery rates, the result indicates that the delivery mechanism was triggered by cooperative interactions of the peptide. On the basis of the cooperativity constants a new molecule composed of an intramolecular dimer of r_9 showed an improved rate of delivery. The monomer and dimer both have relatively fast rates of uptake, but by using the dimer to deliver cargo the enhancement of the delivery rate could provide a good solution for drug delivery. Quantitation of the CPP is carried out in these experiments. This allowed the exact calculation of the uptake in terms of concentration of r_9 and cargo.

Chapter three explores the role of endosomal acidity with respect to the uptake of polyarginine peptides. The acidification and maturation of endosomes is considered to be a necessary step in the delivery process of polyarginine peptides. By employing an inhibitor of vacuolar-ATPases and the acidification that is characteristic of endosome maturation, there is noticeable increase in the delivery rate of polyarginine peptide to the cytosol. Endosomes containing polyarginine peptides linked to pH sensitive fluorescent dyes become acidic over time, and occasionally are seen to abruptly disgorge their contents in real-time as well. Intracellular calibrations of the dye allowed accurate measurement of the pH of the endosomes containing the peptide and indicate that some peptides do remain in endosomes over time and do not escape to the cytosol.

In chapter four a polyarginine peptide is compared to another cell delivery molecule: a guanidinylated transporter. This chapter compares the efficiency of these molecules by their delivery rates using FACS and Fluorescence Microscopy.

Chapter five describes a short study of various pharmacological agents and their affect on the delivery rate of a polyarginine peptide. These agents are understood to affect different components of the macropinocytosis pathway of uptake, but were implicated to perturb CPP peptide uptake. These experiments either indicated that r_9 does not follow only one route of endocytosis or that there are several ways to by-pass certain inhibitory components of the endocytic machinery.

Table 1.1 – Examples of Amphipathic and Cationic cell-penetrating peptides. Peptides are organized by increasing charge.

Cell penetrating peptide	Charge	Peptide Sequence
Amphipathic peptides		
MAP	+4	KLALKLALKLALALKLA
Transportan	+4	GWTLNSAGYLLGKINLKALAALAKKIL
Pep-1	+5	KETWWETWWTEWSQPKKKRKV
pVec	+6	LLIILRRRIRKQAHAHSK
Penetratin	+7	RQIKWFQNRRMKWKK
Cationic peptides		
TAT	+8	YGRKKRRQRRR
R_9 (D- or L-isomer)	+9	RRRRRRRRR
R_9-TAT	+9	GRRRRRRRRRPPQ

References

1. "Drug Delivery and Targeting for Pharmacists and pharmaceutical Scientists" Edited by Anya M. Hilery, Andrew W. Lloyd and James Swarbrick, published by Taylor & Francis, Inc. © 2001

2. Wim, H., De, Jong, and Borm, Paul J.A., "Drug delivery and nanoparticles: Applications and hazards." Int J Nanomedicine. 2008 June; 3(2): 133–149.

3. A.D. Frankel and C.O. Pabo, "Cellular uptake of the tat protein from human immunodeficiency virus," Cell 55 (1998), pp. 1189–1193.

4. Green, M., and P. M. Loewenstein, Autonomous functional domains of chemically synthesized human immunodeficiency virus tat trans-activator protein. Cell 55(6): (1988) 1179–1188.

5. D. Derossi, A.H. Joliot, G. Chassaing and A. Prochiantz, The third helix of the Antennapedia homeodomain translocates through biological membranes, J. Biol. Chem. 269 (1994), pp. 10444–10450.

6. E. Vives, P. Brodin and B. Lebleu, A truncated HIV-1 Tat protein basic domain rapidly translocates through the plasma membrane and accumulates in the cell nucleus, J. Biol. Chem. 272 (1997), pp. 16010–16017.

7. Wadia, J. S., R. V. Stan, and S. F. Dowdy, 2004. Transducible TAT-HA fusogenic peptide enhances escape of TAT-fusion proteins after lipid raft macropinocytosis. Nat. Med. 10(3):310 – 315.

8. Tunnemann, G., R. M. Martin, S. Haupt, C. Patsch, F. Edenhofer, and M. C. Cardoso, 2006. Cargo dependent mode of uptake and bioavailability of TAT containing proteins and peptides in living cells. FASEB J 20 (11):1775–1784.

9. Fischer, R., Fotin-Mleczek, M., Hufnagel, H. and Brock, R. "Break on through to the other side – Biophysics and cell biology shed light on cell-penetrating peptides." Chembiochem 6, (2005) 2126-2142.

10. Pooga, M., Hallbrink, M., Zorko, M. & Langel, U. Cell penetration by transportan. FASEB J. 12, 67–77 (1998).

11. Mangoni, Maria, "Host-defense peptides: from biology to therapeutic strategies. Cell. Mol. Life Sci. (2011) 1-3.

12. Pujals, S. Giralt, E. "Proline-rich, amphipathic Cell-penetrating peptides." Adv. Drug Delivery Reviews. 60 (2008) 473-484.

13. Crombez, L., Aldrian-Herada, G, Konate, K., Nguyen, Q.N., McMaster, G.K., Brasseur, R. , Heitz, F., Divita, G., "A new Potent Secondary Amphipathic Cell-penetrating peptide for siRNA Delivery to Mammalian Cells." Mol. Therapy, 1 (2009) 95-103.

14. Wender, P.A., Mitchell, D.J., Pattabiraman, K., Pelkey, E.T., Steinman, L., and Rothbard, J.B. "The design, synthesis, and evaluation of molecules that enable or enhance cellular uptake: peptoid molecular transporters." PNAS 97 (2000), 13003-13008.

15. Khalil, I.A., Kogure, K., Futaki, S., Harashima, H. "Octaarginine- and octalysine-modified nanoparticles have different modes of endosomal escape." J. Biol. Chem. 281 (2006), 3544-3551.

16. Chauhan, A, Tikoo, A., Kapur, A.K., and Singh, M. "The taming of the cell penetrating domain of the HIV Tat: myths and realities." Journal of Controlled Release 117 (2006), 148-162.

17. Lagerholm, B.C. "Peptide-mediated intracellular delivery of quantum dots." Methods Mol. Biol. (2007) 374, 105-112.

18. Holm T, Andaloussi SE, Langel U. "Comparison of CPP uptake methods." Methods Mol Biol. 2011;683:207-17.

19. Thierry AR, Abes S, Resina S, Travo A, Richard JP, Prevot P, Lebleu B. "Comparison of basic peptides- and lipid-based strategies for the delivery of splice correcting oligonucleotides." Biochim Biophys Acta. 2006 Mar 1758(3):364-74. Epub 2005 Nov 18.

20. Wadia, J.S. and Dowdy, S.F. "Protein transduction technology." Curr. Opinion in Biotechnology 13, Issue 1 (2002) 52-56.

21. Oehlke, Johannes, et al. "Cellular uptake of an [alpha]-helical amphipathic model peptide with the potential to deliver polar compounds into the cell interior non-endocytically." Biochimica et Biophysica Acta 1414 (1998): 127-139.

22. Burlina, F, et al. "Quantification of the Cellular Uptake of Cell-Penetrating Peptides by MALDI-TOF Mass Spectrometry." Angewandte Chemie Internationale Education (2005): 4244-4247.

Chapter Two

Fluorescence-based study of the mechanism, kinetics, and quantitation of polyarginine CPP cytosolic delivery

Abstract

Drug delivery continues to be a costly challenge for pharmaceutical companies. Candidate therapeutics are often dismissed because of the inability to create a formulation that will enable them to be effectively delivered to the site of action inside the cytosol and nucleus of cells. In the past 20 years cell penetrating peptides (CPP) have become a key area of study for the therapeutics and research industry because of their unique feature to be internalized inside cells by endocytosis even when attached to large charged molecules. Although generally the extensive positive charge on most CPPs is considered to be the unique feature that helps them gain entry to cells by mediating a close cell membrane interaction, there is little known about the efficiency of CPP cytosolic delivery or what allows the peptide to break free of vesicles and endosomes that sequester the peptides from the cytosol. Utilizing a unique FRET based assay the delivery efficiency of an example CPP, a nonamer of (D)-arginine (r_9), is quantitatively measured. Additionally, the r_9 CPP entry mechanism and dynamics is probed for cooperativity in the mechanism, which is validated by engineering an intramolecular dimer of r_9 which enhances uptake kinetics 3-15 fold. Together the measurement of r_9 CPP and the enhancement of cytosolic delivery with a dimer of r_9 provides evidence that r_9 may form dimers to assist in breaking free of the endosomes that sequester the peptide. Thus, to enhance delivery of normally non-penetrating molecules this evidence suggest that using dimers of CPPs could enhance uptake as much as 15 fold.

Introduction

For CPPs to be useful as a drug and therapeutic delivery method it is dependent on their ability to reach a specified location within the cell. Most therapeutic targets are in the cytoplasm and any anti-sense gene therapy must be able to enter the cytosol or the nucleus. Furthermore the process must be relatively quick to ensure that the molecule is not degraded or repackaged for exocytosis in the transport pathway.

Polyarginine CPP, due to the high level of guanidinylation, has demonstrated an excellent ability to be internalized into cells through endocytosis as compared to other forms of cationic peptides.[1] However, the peptide localization within the cells has been ambiguous. Researchers have not been able to quantify the peptides' ability to deliver cargo specifically to the cytosol with most current methods.[10]

Methods that have been developed can be categorized as biological or chemical. Biological methods often depend on a secondary response from the cell to determine localization. Visual clues of the cell response, induction of apoptosis, non-proliferation, splice correction, interfering oligonucleotides, Cre-recombinase integration of a functional gene are all ways that CPP delivery is evaluated.[15] Chemical methods aim to provide an exact number or a relative number for the delivery of the CPP molecules. HPLC, quantitative spectrofluorimetry, and mass spectrometry all provided more analytical and quantitative measurement of the CPP and its cargo once removed from the biological system. Some methods can combine biological and chemical measurements to determine localization and quantify the peptide in a cellular compartment, but neither of these method categories has been able to provide real-time quantitative and localization information.

Specifically for the study of CPP localization, fluorescence has become very popular for its high sensitivity and the ability to monitor the cell in real-time. Another technique that is very useful is fluorescence resonance energy transfer (FRET). FRET becomes useful especially in this circumstance, as it is dependent on bringing two components in close proximity in order to produce a resonant energy transfer and thus an optical response that can be measured quantitatively. This fundamental principle can be exploited to evaluate if a peptide molecule is within proximity of another independent molecule. In the cell system, initially the two components can be separated by a cell membrane and only through a cell process that brings them together can a resonant energy transfer process occur.

A FRET application to approach the question of CPP delivery was developed by the Tsien lab.[16,17] This method conjugates the CPP with an initially non-fluorescent acceptor molecule called fluorescein biarsenical hairpin binder (FlAsH) and requires the cytosolic and nuclear expression of a cyan fluorescent protein encoded on the carboxyl terminus with four cysteines (CFP-4Cys) to which FlAsH can specifically bind. FRET from CFP to FlAsH provides a continuous assay of the amount of FlAsH that has reached the cytosol and nucleus. [17]

Here we present this FRET method as an essential tool to determine the efficiency of delivery of polyarginine CPP specifically to the cytosol. Furthermore, any modifications to the polyarginine scaffold can be quickly evaluated for its ability to improve or diminish the delivery efficiency of the CPP. The efficiency of the delivery of monomeric polyarginine (r_9) and a dimeric form of r_9 are described here and evaluated by

the FRET method of measurement. A unique method for quantification of the peptide via calibration of the CFP in the FRET system is also presented.

Results and Discussion

Optimizing conditions to monitor delivery of r_9 CPP. Fluorescence and FRET is a highly sensitive method of detection, but within the cell other variables can affect the sensitivity of the fluorescence response. It is important to use molecules that cause the least perturbation to the cell in order to minimize artifacts.[33]

To guarantee the most sensitive response while ensuring that the cell was minimally perturbed by the fluorescent protein and 4Cys tag, the protein and tag sequence was selected based on photostability and FRET efficiency. The mECFP protein sequence shows the best photostability of the commonly used CFP proteins (CyPet, Cerulean, mCFP) and additionally is a stable monomer.[33] The 4Cys tag was selected based on the optimal FRET efficiency to the FRET acceptor for CFP, FlAsH, a fluorescein-based bi-arsenical dye. Several sequences were determined to have optimal binding efficiency to FlAsH as measured by competitive chelation or binding to FlAsH. British Anti-Lewisite (BAL) is another term for 2,3-dimercaptopropanol. BAL can strip the FlAsH away from binding the 4Cys target sequence by efficiently binding the arsenic groups on FlAsH. The disadvantage of BAL is that it is also very toxic to cells. With this caveat in mind, the 4Cys sequence was selected for optimal FRET efficiency and lower affinity of binding to FlAsH, which would require less concentrated BAL to strip FlAsH from the 4Cys. For our purposes the 4Cys sequence that was determined to

produce the best FRET efficiency was –CCPGCC— as indicated by measurements published in Martin, B.R., *et al*.[17,18] The –CCPGCC— sequence produces ~75% quench of the CFP (unpublished results from B.R. Martin) while only requiring 5mM BAL for unbinding FlAsH. It should be noted that a more optimal sequence for FlAsH binding includes modifying flanking regions of the tetracysteine (*ie*.—FLNCCPGCCMEP—) but this sequence has a slightly lower FRET efficiency of ~65% and also requires twice the BAL concentration for FlAsH to unbind the tetracysteine sequence. Finally, the FlAsH molecule used was in actuality 5-carboxy-FlAsH, which contains an additional carboxyl group that allows for a handle to conjugate to the r_9 peptide (Fig. 2.1). This additional carboxyl groups did not create any observable variations to the fluorescent properties of the dye.

Figure 2.2 demonstrates the FRET mechanism between CFP-FlAsH. Upon FlAsH binding to CFP-4Cys (Fig. A1.1), CFP loses most (~75%) of its fluorescence by FRET to FlAsH (Fig. 2.2).[17,18] Adding BAL removes FlAsH from CFP-4Cys and recovers the CFP fluorescence (Fig. 2.2). The reduction of the CFP fluorescence specifically monitors and measures r_9 CPP cytosolic and nuclear delivery kinetics without interference from r_9 bound to the intracellular or extracellular leaflet of the membrane or within endosomes (Fig. 2.2). Recovery of CFP fluorescence by competitively binding FlAsH with BAL, ensures that the measured quench is not due to photobleaching or non-specific interactions. The lower concentration of BAL slows cell toxicity during the recovery phase that completes the experiment. As cytosol expressed CFP-4Cys quenched, it indicates the delivery of r_9-FlAsH to the cytosol (Fig. 2.3).

Figure 2.3 depicts CFP-4Cys expressing HeLa cell quenched over 65 minutes by the delivery of r_9-FlAsH at an extracellular concentration of 2 μM. Because there has never been an exact quantification of the total concentration of peptide that could enter the cytosol it was necessary to use a sensitive and fast binding molecule, while ensuring that the cell could survive washing with BAL.

r_9 is delivered to the cytosol at sub-micromolar concentrations. Because of the high cost of therapeutic drugs, insolubility, and poor biodistribution drug delivery is a critical component of drug development.[32] If drugs can be delivered efficiently then the dosage can be reduced (improved efficacy), which also reduces the probability of side effects and adverse health effects related to treatment. Thus, a heavy burden is placed on a drug carrier to deliver a therapeutic efficiently to the site of action, while ensuring no toxicity or lower toxicity to the system. This challenge can be approached in two ways: a highly potent drug with an inefficient carrier may still provide a reasonable result or a highly efficient carrier combined with a less potent drug or a drug mixture could provide just as good of a result as a high potency drug. The latter may be preferred to minimize toxicity from over dosage of a potent drug. To address this latter approach, we tested a range of concentrations of r_9-FlAsH to determine how efficiently the peptide can deliver a molecule to the cytosol. Additionally, it was a secondary interest to determine the limits of the dynamic range of the FRET assay.

In order to determine the range in which this method would be useful for r_9-FlAsH, concentrations from sub-micromolar, 0.25 μM, to 2.5 μM were applied to CFP-4Cys expressing HeLa cells and quench of CFP was monitored by fluorescence

microscopy in individual cells over the course of the 60 minutes (Fig. 2.4). Applying 0.25 μM r_9-FlAsH to the cells results in a slow quench over the 60 minute range equivalent to 10% of the maximum measurable change in CFP fluorescence. At 0.75 μM of r_9-FlAsH application the quench was reached almost 20% of maximum over 60 minutes. The CFP-4Cys quench continued to increase as the concentration of applied r_9-FlAsH increased, up to 80% completion at 2.5 μM application of r_9-FlAsH. On average, within the 0.25 μM – 2.5 μM range the CFP within cells was not maximally quenched (Fig. 2.4), but at higher concentrations of applied r_9-FlAsH, intracellular CFP fluorescence quenched quickly, but appeared to show signs of toxicity and cell death. It is hypothesized that cell death could be a result of direct permeation of the outer membrane resulting in the extrusion of the cell interior fluid. This destabilization of the cell membrane can result in cell death. Although this could be a useful side effect of r_9 in killing diseased cells, for the purposes of this study it was not the pursued result as it would not achieve any findings that would help elucidate the mechanism of uptake or cell entry. Furthermore, that level of dosage is not feasible in clinical practice.

Here it is important to note a caveat that was discovered while developing this assay to be useful at low concentrations. FlAsH as well as r_9 are both highly prone to adhere non-specifically to surfaces. Plastic surfaces are hydrophobic surfaces particularly well-suited to allow non-specific adhesion and aggregation. When initial tests were completed to note how much of the peptide remained in the soluble portion of the plastic dishes, it was noted that almost 25% was lost to non-specific adhesion to the well walls within the first few minutes of adding the peptide to the dish (Fig. A1.2, A1.3). This phenomena was observed in dishes with cells as well. The non-specific interactions

were amplified for low concentrations of r_9-FlAsH but for high concentrations the non-specific binding did not have as much of an effect in the soluble concentration. To combat this, the assay was modified to include a "replenish" step in which all of the soluble volume was removed and replaced with the same concentration of r_9-FlAsH. This step resulted in measureable uptake for low concentrations especially.

Rate of r_9 cytosolic delivery indicates cooperativity. The normalized change in CFP fluorescence due to r_9-FlAsH binding CFP-4Cys indicated that as extracellular concentration of r_9-FlAsH increased from 0.25 μM – 2.5 μM the rate of CFP-4Cys quench increased in a non-linear fashion (Fig.2.4). The non-linearity is more clearly noted when the rate of change of CFP fluorescence is plotted against the concentration of applied r_9-FlAsH (Fig. 2.4). There was less than 10% change in the rate of delivery of r_9 peptide from 0.25 μM – 0.75 μM, but the rate of uptake at 1.0 μM increased to 4x greater than the slowest rate from 0.25 μM to 0.75 μM then increased linearly until 2.0 μM r_9-FlAsH, and began to have a more steady pace at concentrations greater than 2.0 μM. To avoid any error in the rate calculation from complete saturation of the CFP-4Cys sites within the cell the rates were taken within the first 20 minutes of the uptake experiment (post r_9-FlAsH addition). Within a 20-minute time frame the concentrations tested were unable to completely quench CFP.

Figure 2.5 depicts a model to explain the non-linearity that is observed in the uptake of r_9-FlAsH. Two assumptions are made; (1) all peptides must be endocytosed to release into the cell and (2) once endocytosed there are only 2 fates, to be sequestered or to be released. It is hypothesized that at low concentrations the peptides may partition at low density/endosome into a majority of the endosomes and only a minority of

endosomes retain a high density/endosome of internalized peptide. To result in breakage and release of their contents into the cytosol the peptide must be at high density. As extracellular concentrations increase, peptides partition at high density into a majority of the endosomes and thus a majority of the endosomes release their contents into the cytoplasm and a minority of endosomes sequesters the peptides. There is a limitation to this hypothesis that is apparent at the highest concentration of r_9-FlAsH that is added to the outside of the cell. As the concentration increases the delivery rate begins to reach an upper limit for the delivery rate. With respect to this consideration and the limitation on the rate, we propose that there could be two possibilities. One possibility is that there is a physiological limitation on the intrinsic rate of endocytosis and recycling of vesicles and membrane. A second possibility is that the limitation is a result of changes in the biochemistry of the endosomes encapsulating the r_9 peptide preventing the peptides from escaping the endosome. It is established that in mammalian cells, vesicles are acidified by vacuolar proton pumps (vacuolar ATPases)[3,11] within endosomes. It is unlikely that the D-peptides are being broken down by endogenous peptidases and some CPPs (TAT, penetratin) are released more quickly by endosomal acidification,[12] but there may be a different mechanism for polyarginine peptides escape mechanism at low pH that results in endosomal sequestration of the peptides.

r_9 delivery to the cytosol is enhanced by intramolecular dimerization. The indication of non-linearity in r_9 cytosolic delivery suggested that there is a cooperative mechanism affecting the delivery step of r_9. Aggregation or clustering has been proposed as a mechanism by which peptides are clustered by surface HSPGs[26,27], however, it has not been emphasized for endosomal release. Figure 2.6 diagrams a model of bi-molecular

uptake or dimerization that maybe necessary for cytosolic delivery of r_9 and it was hypothesized that if the r_9 can be engineered to cis-dimerize then the rate of delivery would increase by nature of the same density model of release. This hypothesis was tested in other CPP molecules and analogs that showed branched or multimeric molecules showed improved uptake into cells.[28,29] To test this hypothesis Sigma Plot 10 (Systat Software, Inc., Point Richmond, CA) dynamic fit wizard tool was used to fit the data of the delivery rate of r_9 using 3-parameter Hill Function. From curve fitting of two experiments the and the standard error of the independent Hill coefficients, the average Hill coefficient and error was found to be 2.02 ± 0.38, which provided good evidence that the scheme of escaping endosomes rapidly may require association or aggregation of the independent molecules of r_9. The result of the Hill coefficient appeared to provide support for the proposed model of the mechanism (Fig. 2.6). A FlAsH-labeled dimer of r_9 was synthesized (Fig. 2.1) to test if the bi-molecular hypothesis for the uptake mechanism for monomeric r_9 could enhance the rate of cytosolic delivery. The intramolecular dimer rapidly enhanced the rate of delivery and by applying the same curve fitting algorithm to the cytosolic delivery rate of the intramolecular dimer of r_9 resulted in a Hill coefficient of 0.98 ± 0.36 (Fig. 1.6).

Although dimerizing r_9 improves the cytosolic delivery efficiency at all concentrations from 0.25 μM to 3.0 μM, the rate at lower concentrations showed and average 8x improvement while at the higher concentrations only 3x improvement. Furthermore, the measurement and the curve fitting methods appear to indicate that the delivery process becomes more linear than sigmoidal as the concentration of the dimerized r_9 increases. However, linearity cannot be concluded because of the intrinsic

limit on the dynamic range of the assay. Although, investigations show evidence that at very high concentrations of r_9 and other CPPs cell toxicity is prevelant. Cell toxicity was not observed in the range 0.25 μM and 3.0 μM but may become a problem at much higher concentrations.[30,31]

Mechanistic studies proposed that CPPs aggregate in some way to enhance cytosolic delivery. Dix, A., *et al* found that aggregation of guanidinylated transporters may be a result of the heparin sulfate proteoglycan clusters on the cell outer-membrane. Arguments have also been made to suggest that aggregation on the surface serve to provide a nucleation site for subsequent cellular uptake and that this phenomenon is not limited to arginine polymers.[34-38] Although it is unclear whether it is nucleation on the cell outer-membrane or within the endocytic vesicle, it is clear that oligomerization plays an important role in release of these peptides into the cytosol. Similar to Figure 2.5, Figure 2.6 depicts a mechanism by which the dimerization of the peptides enhances the delivery of peptides. At low concentrations, monomeric peptides may sparsely disperse inside endosomes resulting in a largely sequestered population of the peptides, but interactions between peptides may enhance the release of the peptides as well. Thus in the dimeric r_9 model peptides always have an intramolecular r_9 partner to interact with, thus resulting in an enhanced release even for sparsely partitioned dimeric r_9.

Quantified intracellular delivery of r_9. The rate of delivery and localized concentration of a therapeutic within a target cell becomes important when considering the *in vivo* efficacy of the therapeutic. The delivery of r_9-FlAsH can be measured by correlating the loss of CFP fluorescence with the efficiency of FRET between CFP and FlAsH upon binding using an *in vitro* calibration of CFP concentration and the calculation that 75% of

the CFP Fluorescence can be quenched by FlAsH (Fig. 2.7).[16,17] Several concentrations of purified CFP protein was calibrated in microcuvettes using the same experimental imaging settings used during experiments (Fig. A1.5). A standard curve was used to calculate the concentration of protein within live cells from fluorescent counts emitted from the cell (Figure 2.7). As FlAsH quenches CFP in the cell, using the 75% FRET efficiency and the calculation of the concentration will provide a calculation of the rate of CPP delivery into the cell as a function of concentration. As the applied concentration increases from 0.25 μM to 2.5 μM, the delivery rate of r_9-FlAsH is measured from 52 pM/min to 650 pM/min. The cytosolic delivery rate of r_9-FlAsH begins to taper off at 2.5 μM and 3.0 μM as the system achieves a maximal rate. The r_9 dimer further increases the rate of delivery of the FlAsH cargo by 3 – 15 times (Figure 2.8).

Therapeutic studies aim for an IC_{50} value between picomolar and micromolar range and the data indicate that within this range polyarginine peptides would be useful to deliver small molecules to cytosolic targets within the cell. As monomers r_9 peptides could deliver as much as 250 pM to 3 nM of a small molecule therapeutic in 5 minutes, but as intramolecular dimerized molecules the delivery in the same amount of time could be 1.5 nM to as much as 13 nM.

Conclusion

CPPs continue to be an active subject of research although there has been very few methods to draw conclusions regarding their efficiency of delivery and effectiveness in a live cell. Using fluorescence-based measurement allows for sensitive detection of

the most efficient peptides that can enter a cell or tissue, but further information on localization can be a challenge when the basis is only cell morphology. CFP-FlAsH FRET becomes a useful method with added proximity information and temporal resolution. Using a CFP-FlAsH FRET assay the preceding results showed that the cytosolic delivery rate is concentration dependent and the rate of delivery of r_9 CPP can be as low as 52 pM/min but as high as 650 pM/min. Furthermore, the non-linear rate measurements led to a re-engineering of the peptide scaffold to form an intramolecular dimer. The dimer increases the rate of delivery to as much as 13 nM of the cargo to the interior of the cell in 5 minutes. This unique FRET assay enabled us to observe the time-resolved cytosolic delivery rate of r_9 CPP live.

Materials and Methods

Peptide synthesis, purification, validation, and fluorophor labeling. Peptides were prepared by standard solid phase Fmoc (9-fluorenylmethyloxycarbonyl) synthesis methods with NovaSyn® TGR resin. Prior to cleavage the peptide was capped by an acetyl group on the amino termini with 66% acetic anhydride (Sigma), 17% Lutidine base (Sigma), 17% tetrahydrofuran (Sigma), and a catalytic quantity of dimethyl-amino-pyridine (Sigma) at 5x volume of the resin, mixed for 2 hours at room temperature. The peptide is cleaved from the resin by an acidic solution composed of 94% trifluoroacetic acid (TFA, Acros Organics), 2% triisopropylsilane (Sigma), 2% ethanedithiol (Fluka Analytical), and 2% thioanisole (Sigma) and mixed for 2 hours at room temperature to cleave. Upon cleavage the carboxyl terminus attached to the resin is released as an amide. The peptide was composed of acetylated D-lysine, aminohexanoic acid (x), and nine D-arginines (Ackxr$_9$). Once cleaved the peptide was analyzed on an Agilent 1100 HPLC/MS with a Phenomenex Luna® 5 μm C18 100 Å LC Column 250 x 4.6 mm from 10-90% acetonitrile (Sigma) and water mixture with 0.01% TFA at a flow rate of 1.0 mL/min and the peptide mass identified in the positive ion mode at the +3, +4, +5 M+H$^+$ (M/z 569.7, 427.7, 342.3). Preparative purification was carried out on an Agilent 1100 HPLC with a Phenomenex Luna® 5 μm C18 100 Å LC Column 250 x 10 mm from 10-90% acetonitrile (Sigma) and water mixture with 0.01% TFA at a flow rate of 1.8 mL/min.

Similar preparation was used for the dimeric r$_9$, however, it was purified at 5-30% acetonitrile (Sigma) and water mixture with 0.01% TFA at a flow rate of 1.0 mL/min and

the peptide mass identified in the positive ion mode at the +3, +4, +5 $M+H^+$ (M/z 569.7, 427.7, 342.3). Preparative purification was carried out on an Agilent 1100 HPLC with a Phenomenex Luna® 5 μm C18 100 Å LC Column 250 x 10 mm from 10-90% acetonitrile (Sigma) and water mixture with 0.01% TFA at a flow rate of 1.8 mL/min.

Succinylated-carboxy-FlAsH$(EDT)_2$ obtained from Dr. Stephen Adams, was mixed with 1.5 eq. purified $Ackxr_9$ or Acr_9xkxr_9 in DMSO with 1.0 eq. diisopropylethylamine (Aldrich) and monitored overnight by Agilent 1100 HPLC/MS for completion. The labeled peptide was purified at 10-90% ACN/H_2O (0.01%) at a flow rate of 1.8 mL/min on a Phenomenex Luna® 5 μm C18 100 Å LC Column 250 x 10 mm and identified by M+3, +4, +5 H^+ for the monomer (M/z 799.8, 600.1, 480.4) and M+6, +7, +8, +9 H^+ for the dimer (M/z 653.6, 560.4, 490.5, 436.2).

After FlAsH labeled peptides were purified, samples were lyophilized and dissolved in a minimal amount of DMSO. Peptide-FlAsH was measured by FlAsH absorbance in 0.1N NaOH at 510 nm at an extinction coefficient of 69,500 $M^{-1}cm^{-1}$ on a Varian Cary 3E UV/Vis Spectrophotometer.

Cell Culture. HeLa cells were maintained in Dulbecco's Minimum Essential Medium (Life Technologies) supplemented with 10% fetal bovine serum and 1% penicillin/streptomycin. Cells were passaged when reaching 90% confluency. Cells were plated on #1 glass coverglass-bottom dishes 48 hours prior to imaging into 8-well Nunc Lab-Tek™ Chambered Coverglass (Thermo Scientific).

Transfection of Cells. Transfection solution was prepared with pCDNA3 vector containing CFP-4Cys (Appendix 1) gene insert. Fugene HD (Roche) was used according

to commercial protocol. Cells were transiently transfected 36-48 hours before imaging experiment.

Live cell epifluorescence imaging. FRET Imaging experiments to measure cytosolic delivery of r_9-FlAsH or r_9-FlAsH-r_9 was completed on an Axiovert 200M (Carl Zeiss Micro-Imaging, USA) inverted epifluorescence microscope with a Plan NeoFluar 40x oil immersion objective (1.30 NA). CFP was imaged with a 420/20 bandpass excitation filter, 450 nm dichroic mirror, and 475/40 bandpass emission filter with 1 second exposure and 10% Neutral Density filter. All images were captured with a Photometrics Cascade II 1024 CCD camera (Photometrics, Tucson, AZ). Slidebook 4.0 by (Intelligent Imaging Innovations, Inc.) was used to capture and analyze images.

For standard imaging experiments, cells were imaged in 8-well chambers after being washed 3x with Hanks Buffered Saline Solution supplemented with 2g/L glucose at pH 7.4. CFP-4Cys transfected cells were imaged for up to 15 minutes prior to adding peptide-FlAsH. After the peptide is added in 10 min the well is washed and the peptide is applied again. This is due to peptide-FlAsH non-specifically binding to the plastic surfaces as measured by absorbance (Fig. A1.2 – A1.4).

CFP calibration. ECFP expressed in pRSETB bacterial protein expression vector was purified from *E.*coli after 24 hours time for expression. Bacteria were pelleted and lysed and supernatant was passed thorough a nickel bead column to capture protein by hexahistadine tag on the C-terminus. Washing was carried out with 10 mM imidazole. Purified ECFP was concentrated by 30Kd Centricon concentrating tubes and resuspended

in MOPS buffer (pH 6.5). The protein concentration was calculated using a Varian Cary UV/Vis. Stock concentation was diluted to make 4 separate calibration concentrations. Microcuvettes were flowed for 3 minutes to minimize protein sticking to surfaces. Finally, cuvettes were capped with optically transparent glue and imaged on as epifluorescence imaging protocol dictated. The width of each cuvette and length was calculated to determine the volume and correlated to fluorescence counts for concentration. The camera counts were plotted against the concentration and used for later calculation of the change in CFP-4Cys fluorescence counts and the correlated to the quantitatively delivery of r_9-FlAsH.

Fluorescence data processing. After live imaging cell fluorescence was processed in Slidebook 4.0 (Intelligent Imaging Innovations, Inc. Denver, CO, USA). CFP-4Cys transfected cells were encircled individually and a mask was generated to track the cell over the time course of the experiment. Additionally, a background region was selected in a region without cells. The sum of the raw CFP fluorescence counts were collected for each cell and the background and the area of the cell. The area of the cell becomes important when considering that a cell with greater surface area will have more accessibility to the soluble peptide. The data was exported to a text file and processed rapidly through a Java program (Fig. A1.6) that rapidly read in the text file and calculated the corrected cell counts of each object with the background level of counts to produce an output file of the time, the area, and the corrected cell counts. The counts were further corrected by scaling the area to 1000 μm^2. This number is arbitrary and fluorescence could also be calculated as the mean of the fluorescence counts.

The rate of peptide uptake was calculated by taking the change of fluorescence over the first 20 minutes of the experiment (post-peptide-FlAsH addition). This served to ensure that the concentration of the CFP-4Cys was in sufficient concentration and unsaturated.

Figures

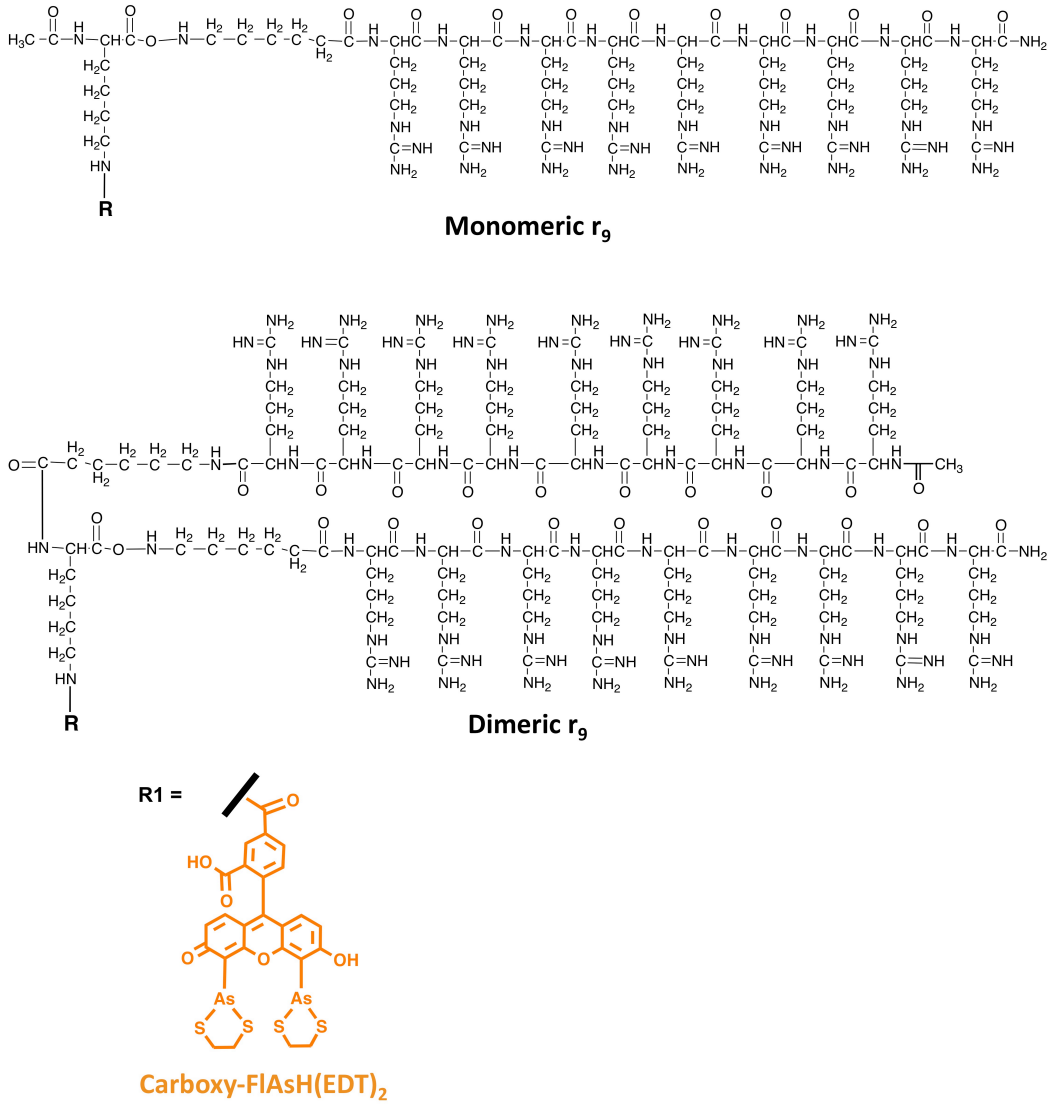

Figure 2.1 – Monomeric and dimeric r_9 Peptide scaffolds used for the study. Carboxy-FlAsH(EDT)$_2$ carboxylic acid was attached via the ε-amine of D-Lysine.

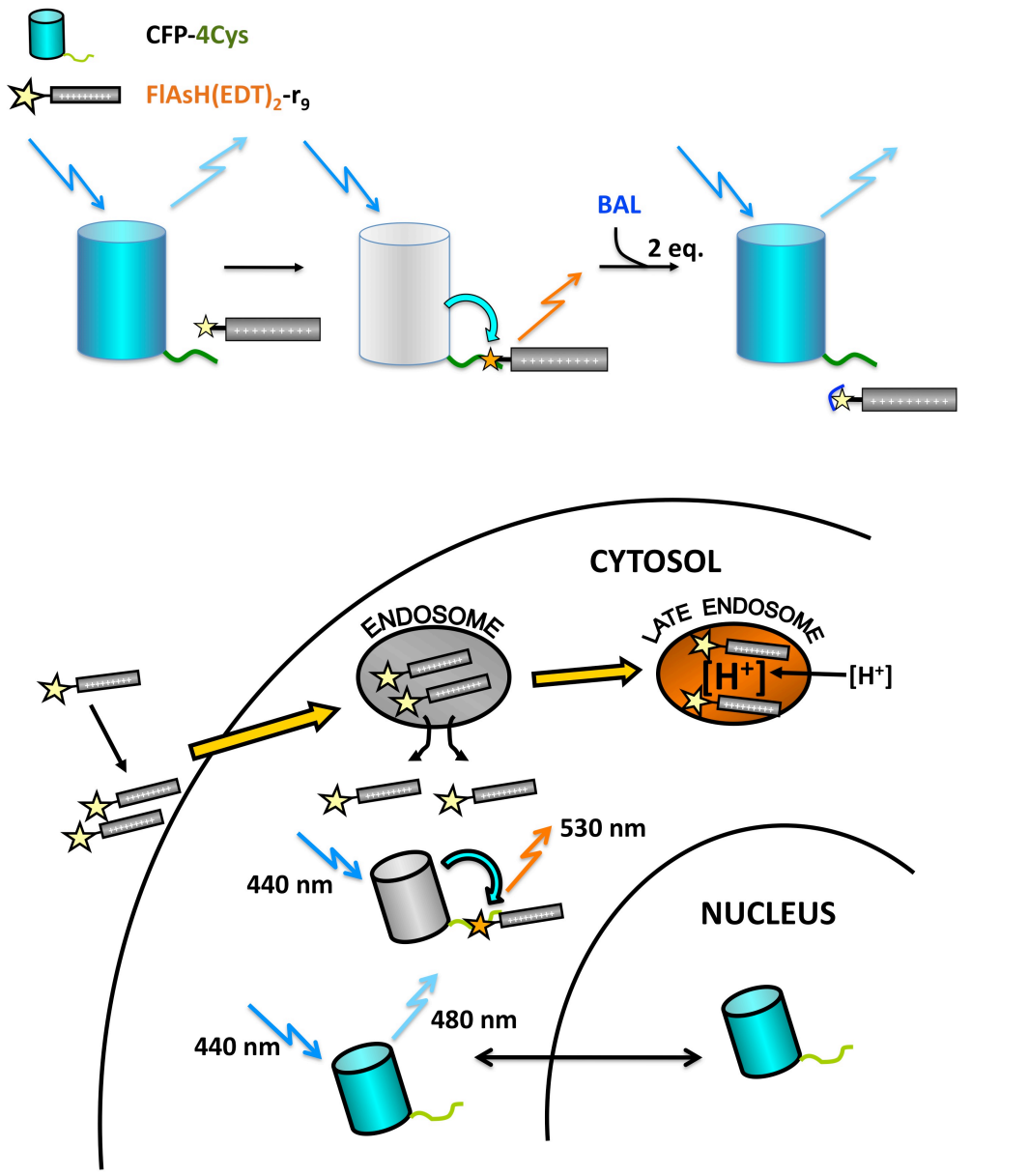

Figure 2.2 – *(above)* Scheme of FRET between r_9-FlAsH interaction with CFP-4Cys resulting in a CFP fluorescence quench and recovery modulated by 2,3-dimercaptopropanol, BAL. *(below)* A cartoon depicting r_9-FlAsH in the extracellular media and the proposed general mechanism of endocytic entry into cells and escape into the cytosol or potential sequestration in late endosomes.

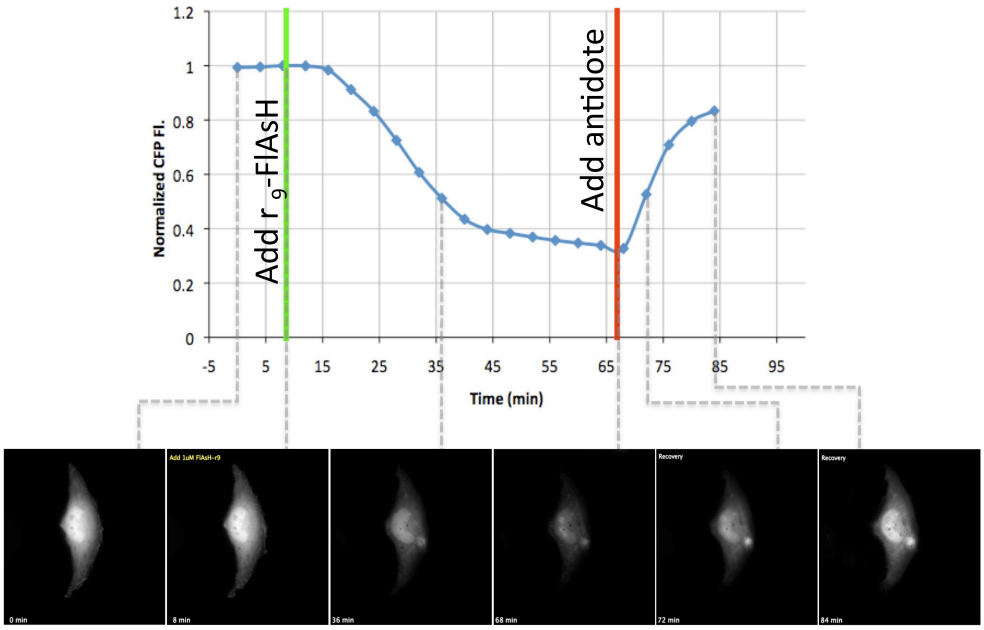

Figure 2.3 – Real-time monitoring r_9 cytosolic delivery to HeLa cells. Timeline of CFP fluorescence quench as r_9-FlAsH (2μM) is delivered to the cytosol. Green line indicates point of r_9-FlAsH addition and red line indicates point of BAL antidote addition, followed by CFP-4Cys fluorescence recovery.

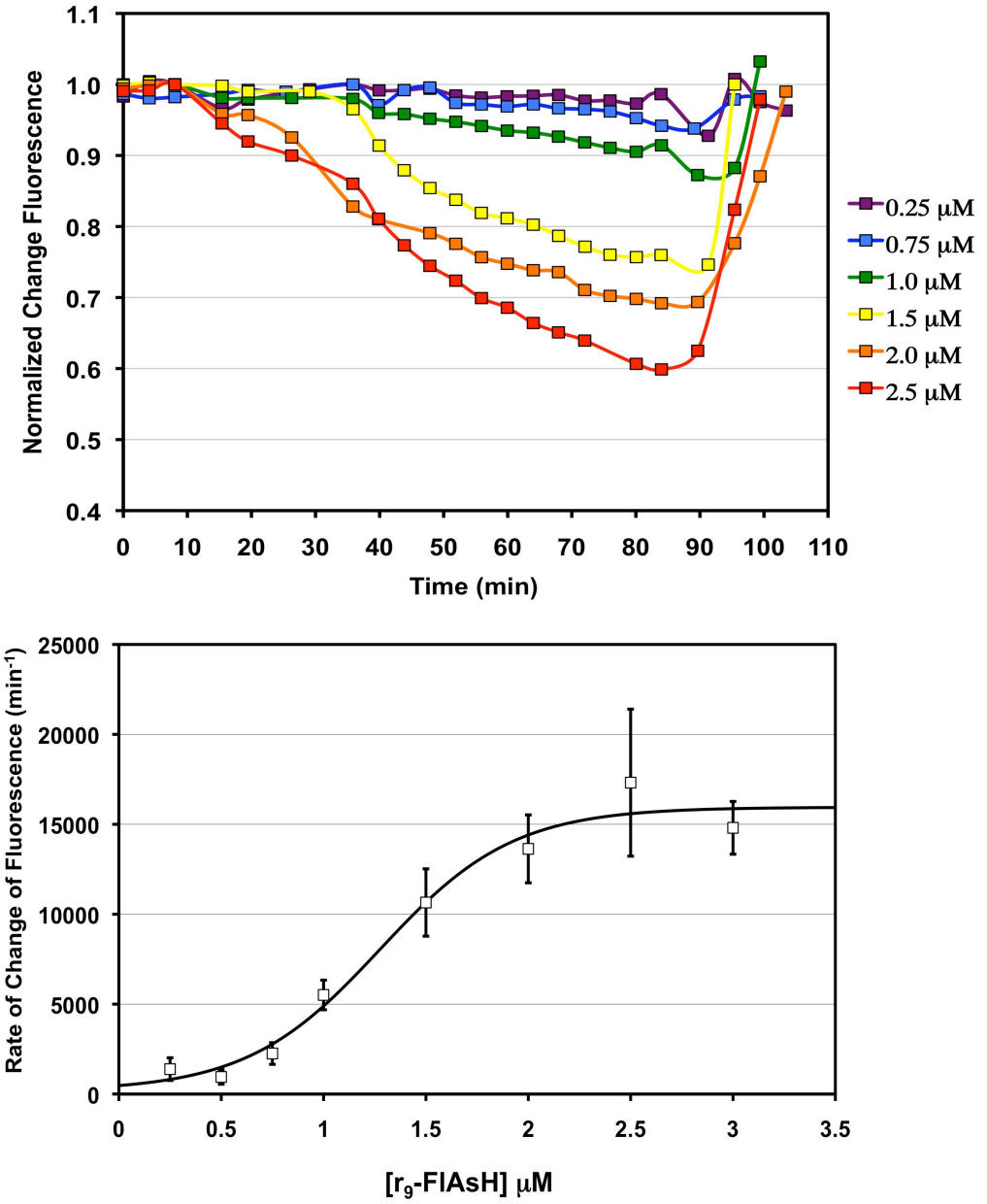

Figure 2.4 – Non-linear relationship of r_9 and rate of cytosolic delivery. (*above*) The time course of 4Cys-CFP expressing HeLa cells is quenched by r_9-FlAsH (0.25 μM to 2.5 μM) delivered to the cytosol. Each trace is an average of 3 separate experiments of 10-20 individual cells. (*below*) Sigmoidal curve fit of the rate of cytosolic delivery of r_9-FlAsH as a function of applied concentration. Each point represents an average rate from three experiments ± SEM.

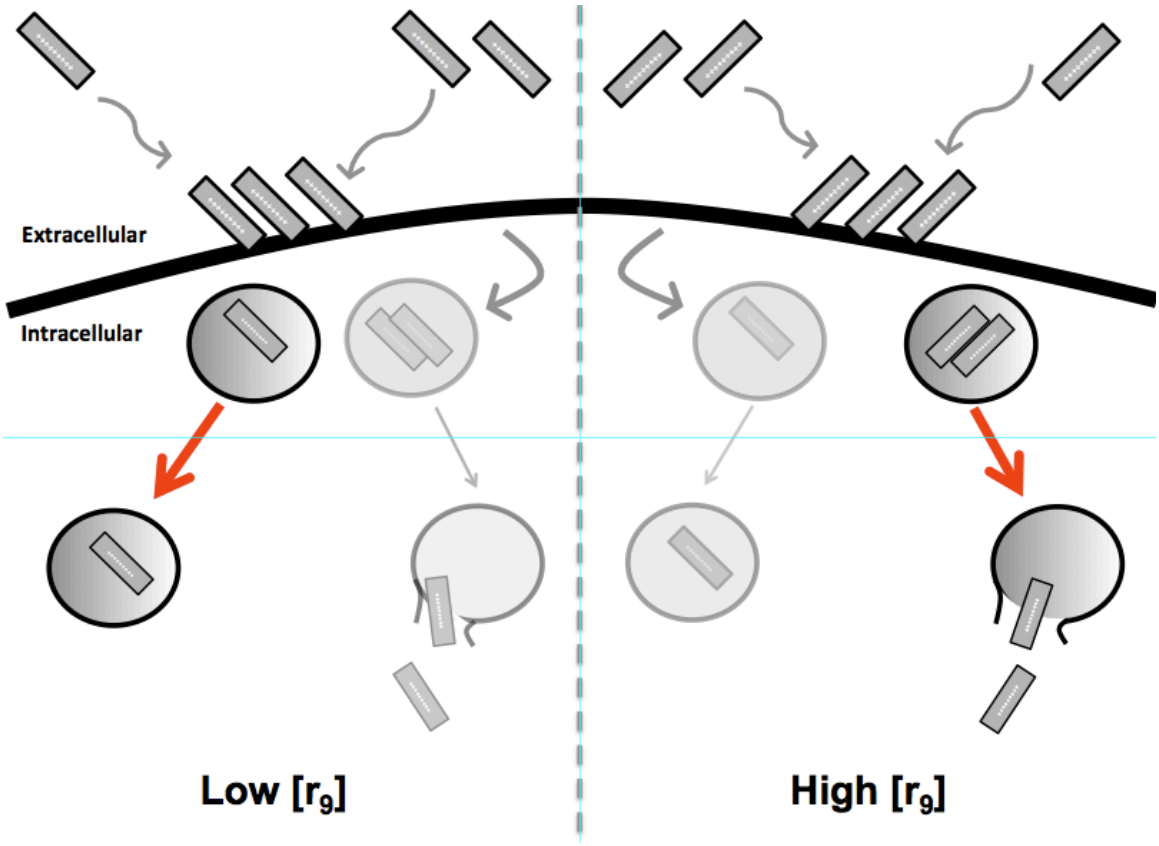

Figure 2.5 – The non-linear relationship of r_9 delivery and concentration may be a result of an intrinsic difference of numbers of r_9 molecules endocytosed. At low concentrations, r_9 peptides partition more sparsely into endosomes, thus resulting in limited release and increased sequestration, whereas, at high concentrations r_9 peptides partition more densely into endosomes and the density is a trigger for release.

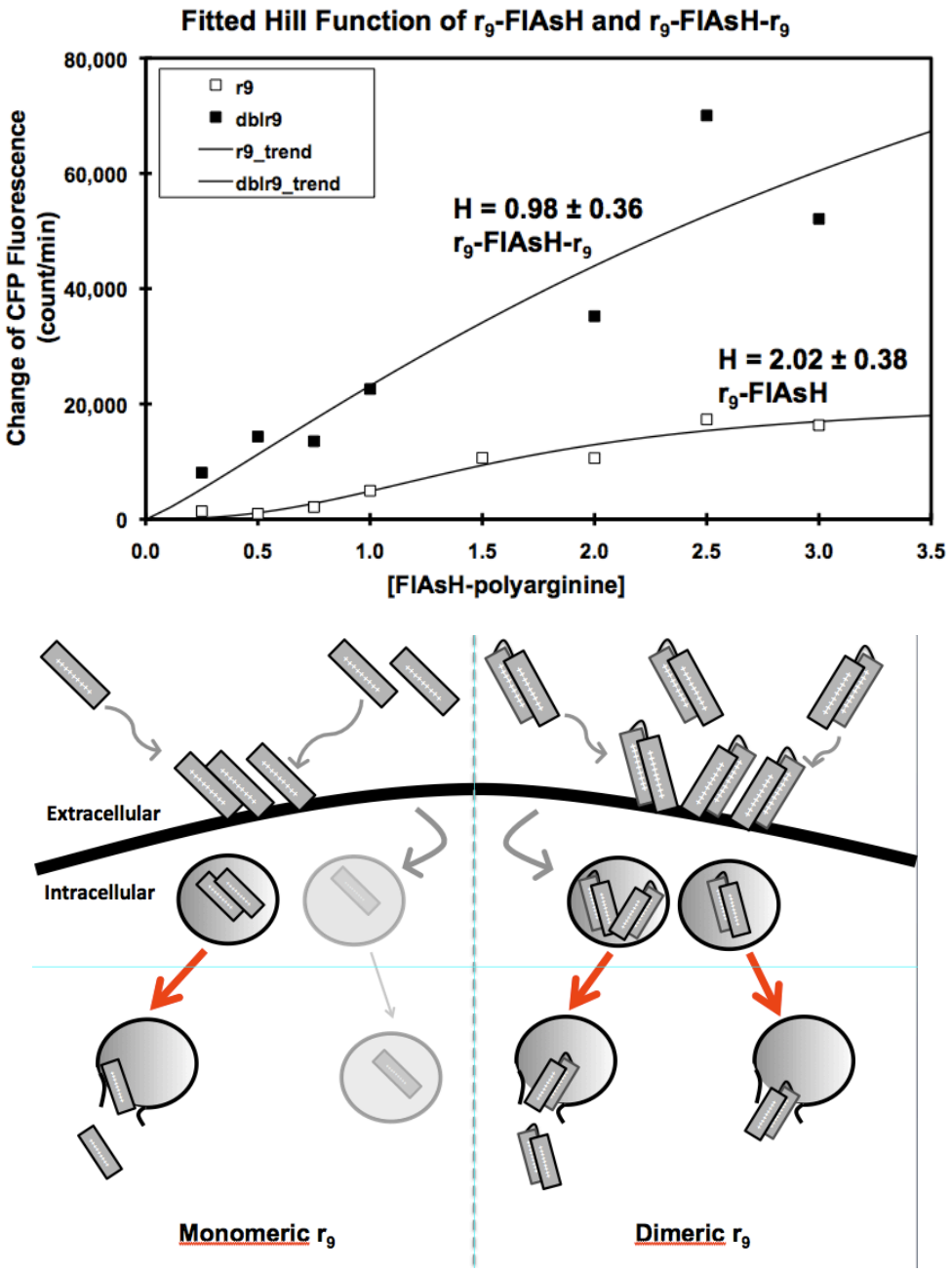

Figure 2.6 – The effect of dimerization of r_9 on cytosolic delivery efficiency. (*above*) Comparison of the rate of delivery of the intramolecular dimer of r_9 (■) and monomeric r_9 (□) as measured by cytosolic delivery of a conjugated FlAsH molecule. Cooperitivity is measured by the Hill coefficient (H ± SEM). (*below*) Cartoon depiction of the proposed r_9 mechnism of entry that requires aggregation of r_9 molecules, which is hypothesized to be expedited by intramolecular dimerization of r_9.

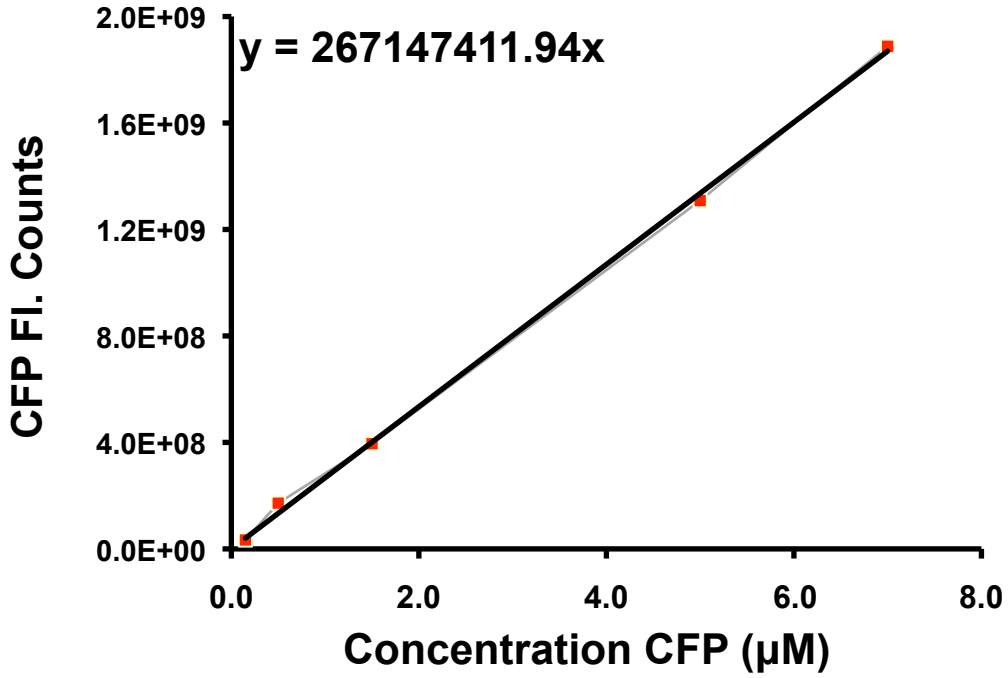

Figure 2.7 – Quantitation of cytosolic concentration of CFP-4Cys.

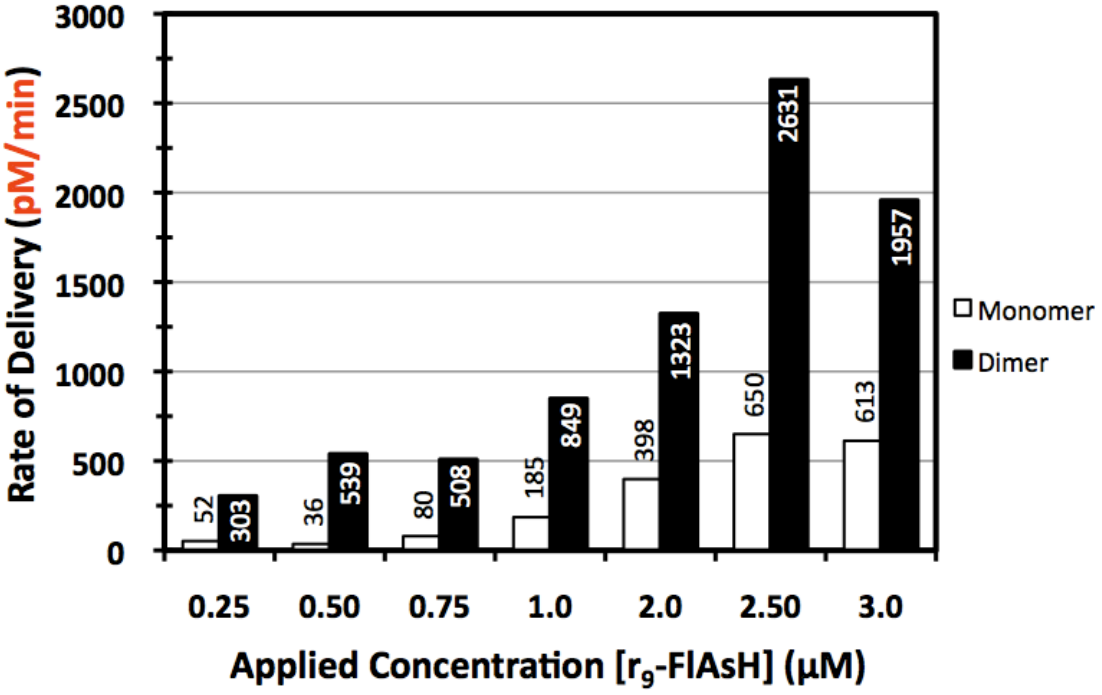

Figure 2.8 – Quantitation of cytosolic delivery of FlAsH-polyarginine.

Acknowledgement

Chapter two is currently being prepared for submission for publication. The dissertation author was a primary author. Co-authors include Dr. Stephen R. Adams, and Dr. Roger Y. Tsien. Thanks is extended to Paul Steinbach for training and assistance with epifluorescence imaging, confocal imaging, and microcuvette calibrations and calculations.

References

1. Wender, P.A., Mitchell, D.J., Pattabiraman, K., Pelkey, E.T., Steinman, L., and Rothbard, J.B. (2000) The design, synthesis, and evaluation of molecules that enable or enhance cellular uptake: peptoid molecular transporters. *Proc. Natl. Acad. Sci. USA 97*, 13003-8.

2. Khalil, I.A., Kogure, K., Futaki, S., Harashima, H. (2006) High density of octaarginine stimulates macropinocytosis leading to efficient intracellular trafficking for gene expression. *J. Biol. Chem., 281*, 3544-51

3. Wadia, J.S., Stan, R.V., and Dowdy, S.F. (2004) Transducible TAT-HA fusogenic peptide enhances escape of TAT-fusion proteins after lipid raft macropinocytosis. *Nat. Med., 10*, 310-315

4. Chauhan, A, Tikoo, A., Kapur, A.K., and Singh, M. (2006) The taming of the cell penetrating domain of the HIV Tat: myths and realities. *Journal of Controlled Release, 117*, 148-162.

5. Lagerholm, B.C. (2007) Peptide-mediated intracellular delivery of quantum dots. *Methods Mol. Biol. 374*, 105-112.

6. Okuyama, M., Laman, H., Kingsbury, S.R., Visintin, C., Leo, E., Eward, K.L., Stoeber, K., Boshoff, C., Williams, G.H., Selwood, D.L. (2007) Small-molecule mimics of an alpha-helix for efficient transport of proteins into cells. *Nat. Methods, 4*, 153-159.

7. Nakase, I., Takeuchi, T., Tanaka, G., Futaki, S. (2008) Methodological and cellular aspects that govern the internalization mechanisms of arginine-rich cell-penetrating peptides. *Adv. Drug Delivery Rev. 60*, 598-607.

8. Tsogas, I., Theodossiou, T., Sideratou, Z., Paleos, C.M., Collet, H., Rossi, J.C., Romestand, B., Commeyras,A. (2007) Interaction and transport of poly(L-lysine) dendrigrafts through liposomal and cellular membranes: the role of generation and surface functionalization. *Biomacromolecules 8,* 3263-3270.

9. Rothbard, J.B., Jessop, T.C., Wender, P.A. (2005) Adaptive translocation: the role of hydrogen bonding and membrane potential in the uptake of guanidinium-rich transporters into cells., *Adv. Drug Deliv. Rev. 57*, 495–504.

10. Aussedat, B., Sagan, S., Chassaing, G., Bolbach, G., and Burlina, F. (2006) Quantification of the efficiency of cargo delivery by peptidic and pseudo-peptidic Trojan carriers using MALDI-TOF mass spectrometry., *Biochim. Biophys. Acta, 1758*, 375–383.

11. Perrais, D., and Merrifield, C. (2005) *Dynamics of endocytic vesicle creation, Developmental Cell, 9,* 581–592.

12. Fischer, R., Fotin-Mleczek, M., Hufnagel, H., and Brock, R. (2005) Break on through to the other side-biophysics and cell biology shed light on cell-penetrating peptides, *Chembiochem, 6*, 2126–2142.

13. Richard, J.P., et al. (2002) *J. Biol. Chem. 278* 585-590.

14. Jones, S.W., et al.(2005) *Br. J. Pharmacol. 145* , 1093-1102.

15. Kaplan, I.M., Wadia, J.S., Dowdy, S.F., (2005) Cationic TAT peptide transduction domain enters cells by macropinocytosis, *Corrigendum to J. Control Release 102,* 247-253.

16. Griffin, B.A., Adams, S.R., Tsien, R.Y., (1998) Specific Covalent Labeling of Recombinant Protein Molecules Inside Live Cells. *Science 281*, 269-272.

17. Adams, S.R. et al. "Imaging the influx of cell penetrating peptides into the cytosol of individual live cells." Handbook of Cell-Penetrating Peptides ed. Ulo Langel ©2006.

18. Martin, B. R., Giepmans, B. N. G., Adams, S. R., and Tsien, R. Y. (2005) Mammalian cell-based optimization of the biarsenical-binding tetracysteine motif for improved fluorescence and affinity, *Nat. Biotechnol. 23,* 1308–1314.

19. Gerasimenko, J.V., Tepikin, A.V., Petersen, O.H., and Gerasimenko, O.V. (1998) Calcium uptake via endocytosis with rapid release from acidifying endosomes. *Curr Biol. 8*,1335-1338.

20. Jones LR, Goun EA, Shinde R, Rothbard JB, Contag CH, Wender PA. (2006) Releasable luciferin-transporter conjugates: tools for the real-time analysis of cellular uptake and release. *J. Am. Chem. Soc. 128*, 6526-6527.

21. Mellman, I. (1992) The importance of being acid: the role of acidification in intracellular membrane traffic. *Journal of experimental biology 172*, 39

22. Valli, M., Sauer, M., Branduardi, P., Borth, N., Porro, D., and Mattanovich, D. (2005) Intracellular pH distribution in Saccharomyces cerevisiae cell populations, analyzed by flow cytometry. *Applied and environmental microbiology, 71*, 1515.

23. Kulkarni, R. P., Mishra, S., Fraser, S. E., and Davis, M. E. (2005) Single cell kinetics of intracellular, nonviral, nucleic acid delivery vehicle acidification and trafficking. *Bioconjug. Chem. 16*, 986-994

24. Tour, O., Adams, S. R., Kerr, R. A., Meijer, R. M., Sejnowski, T. J., Tsien, R. W., and Tsien, R. Y. (2007) Calcium Green FlAsH as a genetically targeted small-molecule calcium indicator., *Nature Chemical Biology 3*, 423-431.

25. El-Sayed, A., Futaki, S., and Harashima, H. (2009) Delivery of Macromolecules Using Arginine-Rich Cell-Penetrating Peptides: Ways to Overcome Endosomal Entrapment, *The AAPS Journal 11*, 13–22.

26. Belting, M., Wittrup, A., and Sandgren, S., "Proteoglycans as Endocytosis Receptors for CPPs." Handbook of Cell-Penetrating Peptides ed. Ulo Langel ©2006.

27. Ziegler A., Seelig J. (2008) Binding and clustering of glycosaminoglycans: a common property of mono- and multivalent cell-penetrating compounds. *Biophys J., 94*, 2142-2149.

28. Angeles-Boza, A.M., Erazo-Oliveras, A., Lee, Y.J. & Pellois, J.P. (2010) Generation of endosomolytic reagents by branching of cell-penetrating peptides: tools for the delivery of bioactive compounds to live cells in cis or trans. *Bioconjug. Chem., 21*, 2164-2167.

29. Futaki, S., Nakase, I., Suzuki, T., Youjun, Z and Sugiura, Y, (2002) Translocation of Branched-Chain Arginine Peptides through Cell Membranes: Flexibility in the Spatial Disposition of Positive Charges in Membrane-Permeable Peptides. *Biochemistry*, 41, 7925–7930.

30. Watkins, C. L., Brennan, P., Fegan, C., Takayaja, K., Nakase, I., Futaki, S., and Jones, Arwyn T., (2009) Cellular uptake, distribution and cytotoxicity of the hydrophobic cell pentetrating peptide sequence PFVYLI linked to the proapoptotic domain peptide PAD. *Journal of Controlled Release, 140*, 237–244.

31. El-Andaloussi, S., Järver, P., Johansson, H.J., Langel, U., (2007) Cargo-dependent cytotoxicity and delivery efficacy of cell-penetrating peptides: a comparative study. *Biochem Journal, 407*, 285-292.

32. Allen, T. M., and Cullis, P. R. (2004) Drug delivery systems: entering the mainstream., *Science, 303*, 1818–1822.

33. Shaner, N. C., Steinbach, P. A., and Tsien, R. Y. (2005) A guide to choosing fluorescent proteins, *Nat. Methods 2*, 905–909.

34. Dix, A. V., Fischer, L., Sarrazin, S., Redgate, C. P. H., Esko, J. D., and Tor, Y. (2010) Cooperative, heparan sulfate-dependent cellular uptake of dimeric guanidinoglycosides., *Chembiochem 11*, 2302–2310.

35. Watkins, C., Schmaljohann, D., Futaki, S., and Jones, A. (2009) Low concentration thresholds of plasma membranes for rapid energy-independent translocation of a cell-penetrating peptide, *Biochem J. 420*, 179–189.

36. Fuchs, S. M., and Raines, R. T. (2004) Pathway for Polyarginine Entry into Mammalian Cells, *Biochemistry, American Chemical Society 43*, 2438–2444.

37. Fischer, R., Fotin-Mleczek, M., Hufnagel, H., and Brock, R. (2005) Break on through to the other side-biophysics and cell biology shed light on cell-penetrating peptides, *Chembiochem 6*, 2126–2142.

38. Tsogas, I., Theodossiou, T., Sideratou, Z., Paleos, C. M., Collet, H., Rossi, J. C., Romestand, B., and Commeyras, A. (2007) Interaction and transport of poly(L-lysine) dendrigrafts through liposomal and cellular membranes: the role of generation and surface functionalization, B*iomacromolecules 8*, 3263–3270.

Chapter Three

Developing fluorescent tools and methods to investigate the role of endosomal acidification and its affect on cytosolic delivery of r_9 CPP

Abstract

Cell penetrating peptides (CPPs) are known to internalize into endocytic vesicles by a non-receptor mediated process. Furthermore, some CPPs are able to escape sequestration in endosomes and release into the cytosol by an unknown mechanism. Although there is consensus that non-receptor mediated endocytosis is the likely mechanism for CPP internalization, details of this process, characterization of the vesicles, or the release of the CPPs inside the cell have not been addressed. Using a nonamer of (D)-Arginine (r_9) as a model CPP the role of acidification of the endosome and its affect on CPP cytosolic delivery is addressed here. r_9 cytosolic release is measured by employing FRET. Measurements indicate that blocking endosome acidification by a specific vacuolar-type H^+-ATPases inhibitor results in an enhanced release of r_9 into the cytosol, implying that increased endosome acidity inhibits cytosolic release of r_9 CPPs. Using a pH sensitive fluorophore it was possible to calibrate the *in situ* pH of HeLa cells and use the measurement to track and measure the pH of the endocytic vesicles containing the pH sensor labeled r_9 CPP. From these measurements and qualitative observations r_9 CPP cytosolic delivery we conclude that r_9 CPP release is more efficient in the neutral pH environment of the endosome.

Introduction

Cell penetrating peptides (CPPs) are able to enter mammalian cells through an active (energy-dependent) internalization mechanism broadly referred to as endocytosis. The process by which CPPs are endocytosed begins with their contact to the cell surface.

The extracellular surface of cell membrane is decorated with various types of glycans, or carbohydrate groups, on lipid head groups or integral, outer leaflet proteins (proteoglycans).[1] Often these glycan groups are negatively charged while CPPs are generally categorized to carry an overall positive charge (arginine, lysine) and can interact with the negatively charged membrane.[1]

CPPs are reported to enter by several endocytic routes to gain entry to the cell interior.[1] CPPs exhibit extensive promiscuity in the uptake pathway and mechanism for escape from vesicles as well. Several groups demonstrated that CPPs do not follow a consistent route of endocytosis, but instead the endocytic route is dependent on polarity, cargo size, surface interactions, and cell type.[1]

Endocytosis and retention inside endosomes is a major functional barrier that keeps CPPs from being broadly useful for therapeutic applications. Several fluorescently labeled CPPs once taken into cells exhibit a punctate appearance within cell.[2,3] Thus it has been concluded that most CPPs are sequestered in endosomes and excluded from the cytosol and nucleus. However, by FRET we can quantitate that the rate of release of polyarginine (r_9) CPPs is moderate and within the range of common therapeutic agents' LC_{50} (Chapter two).

Once CPPs are internalized, the endocytic path is often followed by shuttling particles within the vesicles to specific organelles or for breakdown and absorption. Following endocytosis, vesicles are often combined into larger endosomes and the pH can begin to reduce from neutral pH 7.2 to pH 5.5.[4] Endosomes are then combined with lysosomes or vesicles coming from the trans-Golgi network carrying degradative enzymes, in which the lumen can be as low as pH 4.6.[4] As endosomes combine with

lysozomes, the pH can change rapidly with integral membrane proton pumps rapidly pumping protons into the newly formed large endosome, called a late endosome. Therapeutics attached to a CPP must remain intact and reach the cytosol in order to serve their purpose to treat the cell. It was demonstrated that within the endosome there are a variety of biochemical changes that signal how the endosome should be targeted inside the cell; to an organelle or a fate as a lysosome.[2] Both endosome fates could result in an ineffective drug delivery agent if the ending location is sequestered from the therapeutic target.

One biochemical trigger following endocytosis and merging of an endosome with a lysosome is lowered pH.[2] Lower pH is a result of vacuolar-type H^+-ATPases (V-ATPase) in the endo-lysosomal membrane.[4,5] pH plays a role in the mechanism by which virus particles escape endocytic vesicles as well. pH also is a key feature of lysosomes and thus could lead to decomposition of therapeutics.[4,5]

To improve the confidence and effectiveness of CPPs there must be a better understanding of the biochemical changes in the endosome interior, or lumen that result in the various fates of an endosome. Understanding this process and how it effects the cytosolic delivery process of CPPs will provide a better basis of how CPPs work with cell biochemistry and how to improve CPPs for drug delivery uses.

Results and Discussion

Attempt to develop a FlAsH based pH sensor. There is a strong interest to determine both the efficiency of cell entry and to gain a better understanding of the state of the

peptide within the endocytic environment. In order to accomplish this an optimal reporter must be able to monitor both the delivery efficiency as well as pH. FlAsH was a good reporter for cytosolic delivery efficiency (Chapter two), but is not an optimal fluorescent pH sensor. However, a precursor of FlAsH, so-called FlAsH-O, was expected to be more sensitive to pH (Figure 3.1, see Appendix 1 for synthesis of FlAsH-O). r_9-FlAsH-O showed indications of a variation in the excitation and emission wavelength when imaged by confocal microscopy at 488 nm (M505-610nm) and 532 nm (M560-595 nm) (Figures 3.1), however the excitation and emission wavelengths were not clearly elucidated with pH titrations (Fig. 3.1). A final attempt was made to understand the behavior of the molecule in cells and endosomes with spectral imaging (Figure 3.2). Spectral imaging revealed that there were two distinct peaks that appeared with r_9-FlAsH-O in separate regions of the cell. Although it was apparent that there were 2 different species of the molecule the species could not be isolated or deconvoluted by traditional analytical methods. Additionally, without clear understanding of the molecule and its behaviour it was not clear how to quantify the molecule. This molecule was abandoned due to the ambiguity of the measurements.

SNARF-4F pH sensor *in situ* calibration of pH inside cells. Any method of quantitation inside cells requires a calibration. To investigate the pH of the vesicles inside cells containing the r_9 peptide a ratiometric fluorescent pH sensor, SNARF-4F (5-,6-) carboxylic acid (SNARF-4F), was conjugated to the r_9 molecule so that the peptide could be tracked in a live cell (Fig. 3.4). SNARF-4F is especially useful for cell biology because the pH inside cells shifts within pH 7.2 to pH 5.0, as described for cytosol, early

endosomes, and lysosomes, which is the same range that the ratiometric dye changes its fluorescence emission ratio.

The sensor was calibrated *in situ* within the cell as conjugated to the r_9 peptide. The pH was calibrated using the "null method" from Eisner, D.A., *et al*. using trimethl amine and butyric acid on a confocal microscope and the maximum projection was used to collect the data. Figure 3.5 depicts the calibration curve that was fitted to the individual pH points were. This curve is useful in determining the pH based on the ratio change of fluorescence wavelength at neutral pH to the fluorescence wavelength at acidic pH. With this calibration curve individual endosome pH could be tracked over time.

pH within endosomes carrying r_9 become acidic within 20 minutes. r_9-SNARF-4F peptides applied to HeLa cells were observed by confocal microscopy. Uptake of r_9-SNARF-4F was visible within 10 min. Endocytic vesicles nearer to the outer edge of the cells were visible in mostly neutral form, but vesicles nearer to the center of the cell but excluded from the nucleus were visible in the acidic form (Fig. 3.6). In Figure 3.7 arrows indicate vesicles just prior to bursting, leaving a puff of red that slowly spreads through the cell, and the remaining small green vesicle or the vesicle disappears. It is important to note that some vesicles release some of the r_9-SNARF-4F and a small portion appears to remain in the vesicle as it become acid (indicated by the green fluorescence shift).

Within a 20-minute timeframe most vesicles within the cell shift to the green wavelength of SNARF-4F. In that short timeframe as the vesicles become more acidic the waves or bursts of r_9-SNARF-4F escaping the vesicles slows. It appears that only in the early stages of endocytosis the r_9 can escape the endosomes. As the vesicle becomes

more acidic the r_9-SNARF-4F indicates an increase in the population of sequestered peptides inside vesicles.

Determining Bafilomycin A1 dosage to inhibit V-ATPases. Bafilomycin A1 (BafA1) is a macrolide anti-biotic natural product that was found to specifically inhibit V-ATPases *in vivo* with very high affinity binding. Furthermore, BafA1 was shown to be cell permeable and thus useful for live cell analysis of the acidification of vesicles.[5] In order to utilize BafA1 in the HeLa model used for r_9 CPP analysis a general assay was necessary to determine the concentration of BafA1 that sufficiently inhibits the V-ATPase in the membrane of endocytic vesicles that have merged with late endosomes or lysosomes. Using the intrinsic property of fluorescent acridine orange (AO) to aggregate in acidic organelles it was feasible to determine the minimum amount of BafA1 that would diminish the aggregation. AO will normally fluoresce at green wavelengths (460 nm) but when aggregated in acidic vesicles or organelles it fluoresces at red wavelengths (650 nm) which enables it to be a general marker for acidic vesicles.[5,6]

Figure 3.3 depicts the effect on HeLa cells in response to a range of BafA1 concentrations from 10 nM to 5 μM. 1 hour of treatment with AO in control samples of HeLa cells showed significant aggregation of AO in acidic lysosomes or lysosome-like vesicles. Diffuse green staining was prominent in the cytosol, the nucleus, and slightly brighter green staining in the nucleoli (Fig. 3.3). The red fluorescence from the aggregate AO appears to be morphologically similar to similar stains of the trans-Golgi region of the cell. Lysosomes are reported to be approximately pH 5 and this pH is important for triggering acid hydrolases that are part of the degradation machinery in lysosomes.[4-7] There was no morphological difference or toxicity among any of the controls in the

presence of AO which lends confidence that the cells are not experiencing phototoxicity or chemical toxicity due to the presence or aggregation of AO within acidic vesicles. The experimental samples were treated with BafA1 for 1 hour prior to adding AO. HeLa cells indicated no aggregation of AO with as little as 10 nM of BafA1 up to 1 μM of BafA1. When BafA1 was added at 5 μM cells developed large vacuole-like, hollow, and non-fluorescent vesicles that took 20-90% of the intracellular space in some cells (Figure not shown). This is hypothesized to be a result of slowing or halting in the trafficking process to such a great extant that the cell vacuoles were gorged with fluid from the extracellular media. To avoid the large vacuoles 10 nM of BafA1 was used to minimize any toxicity while obtaining the needed effect from the cells.

Bafilomycin A1 enhances cytosolic delivery rate of r_9. The FRET based measurement described in chapter two was used to investigate the affect of blocking acidification by BafA1 on the delivery rate of the r_9 peptide. Application of BafA1 during the uptake experiment enhanced the delivery rate of 2μM r_9-FlAsH as much 1.5x, but the rate increase at concentrations below 2μM and above 2μM was less than 1x (Fig. 3.8).

It appears from the time-lapse imaging or r_9-SNARF-4F that the peptide releases in the early stages of endocytosis. In these early time points of the uptake mechanism Figure 3.4 indicates that between 10 and 30 minutes at higher concentrations of applied r_9-FlAsH, the fastest change in the delivery rate occurs. This is the same time period within which the r_9-SNARF-4F molecule is observed to be releasing into the cytoplasm of cells. In the first 15 minutes as the pH in the endosomes is decreasing this could play a role to sequester the peptides further rather than, as previous reports suggest, to release the peptide. We can extend this hypothesis to explain the role of BafA1 and the ability to

enhance release or r_9-FlAsH in the early time period of the experiment. By inhibiting the acidification of endosomes with BafA1, thus halting their maturation, the rate of cytosolic release is moderately enhanced. This effect indicated the r_9 peptides were likely becoming more sequestered as endosomes matured. Thus by blocking the pH and inhibiting maturation of the early endosome, peptides were allowed more time to allow for their release from the early endosome. Additionally, it appears that it is unlikely that the peptides are able to release from late endosomes or more acidic organelles (lysosomes).

Conclusion

Research in the field of CPP studies has reached a consensus that the most likely route of uptake is endocytosis. Endocytosis, although an umbrella term for various mechanisms of uptake, results in endocytic vesicles that share certain characteristics. One characteristic that characterizes maturing and matured endosomes is pH. The pH inside endocytic vesicles begins at a neutral state and as newly formed endocytic vesicles are fused with endocytic vesicles or late endosomes already present, V-ATPase pump protons into the vesicle resulting in the rapid acidification of the vesicle. pH is a variable that has not been characterized in CPP uptake. Here we analyzed and characterized the pH inside endosomes by studying a pH sensor labeled CPP. The main goal was to investigate the potential role of pH and its affect on cytosolic release of r_9 CPP from endosomes into the cytosol.

SNARF-4F responds to both neutral and acidic pH within the physiological range (pH 7.4 – pH 5.0) inside endosomes. This unique feature enabled *in situ* calibration of the pH within endosomes thereby enabling the measurement of the pH of vesicles that specifically contained the r_9. The r_9-SNARF-4F CPP was tracked over real-time to observe the pH and localization of the peptide inside the cell. Additionally, using a FRET assay and a specific V-ATPase inhibitor, BafA1, provided a method to study the direct affect of pH on the rate of cytosolic release.

Cytosolic release is the rate limiting step that keeps CPPs from being beneficial to drug delivery. Thus the rate of cytosolic release is of particular interest in the field of CPP research. Inhibiting the acidification of endosomes with BafA1 moderatley enhanced the rate of cytosolic release. This effect indicated the r_9 peptides were likely becoming more sequestered as endosomes matured indicating that it is unlikely that the peptides are released from more acidic organelles and vesicles. This result is in contrast to previous studies with other non polyarginine CPPs that implicated low pH as a trigger for peptide release.[9]

SNARF-4F pH sensor was extremely useful in determining the pH of the endocytic vesicles containing r_9 peptides. r_9 is taken into endocytic vesicles that are acidified from 7.3 to pH 5.5 - 6.0 in over 28 min. This was concluded from real-time images collected showing pH changes in endosomes dropping uniformally in vesicles selected at approximately the same starting pH but in different cells. Additionally, r_9 release into the cytosol is more pronounced at the early stages of endocytosis while the pH is between pH 6.5 and pH 7.0. This was extrapolated from images taken over 35

minutes in which vesicles were seen bursting and leaving behind dimly fluorescent vesicles that slowly indicated an acidic pH change.

From the data collected it appears that r_9 CPP is clearly taken into endocytic vesicles and furthermore, these vesicles are acidified in under 30 minutes. It can be concluded that pH plays an inhibitory role in the cytosolic release, thus peptide release is most efficient in the early timepoints of the uptake mechanism while pH remains neutral.

Materials and Methods

Peptide synthesis, purification, validation, and fluorophore labeling. Peptide was prepared by standard solid phase Fmoc (9-fluorenylmethyloxycarbonyl) synthesis methods with NovaSyn® TGR resin. Prior to cleavage the peptide was capped by an acetyl group on the amino termini with 66% acetic anhydride (Sigma), 17% Lutidine base (Sigma), 17% acetic anhydride (Sigma), and a catalytic quantity of dimethyl-amino-pyridine (Sigma) at 5x volume of the resin, mixed for 2 hours at room temperature. The peptide is cleaved from the resin by an acidic solution composed of 94% trifluoroacetic acid (TFA, Acros Organics), 2% triisopropylsilane (Sigma), 2% ethanedithiol (Fluka Analytical), and 2% thioanisole (Sigma) and mixed for 2 hours at room temperature to cleave. Upon cleavage the carboxyl termini attached to the resin is converted to an amide. The peptide was composed of acetylated D-lysine, aminohexanoic acid (x), and nine D-arginines ($Ackxr_9$). Once cleaved the peptide was analyzed on an Agilent 1100 HPLC/MS with a Phenomenex Luna® 5 μm C18 100 Å LC Column 250 x 4.6 mm from 10-90% acetonitrile (Sigma) and water mixture with 0.01% TFA at a flow rate of 1.0 mL/min and the peptide mass identified in the positive ion mode at the +3, +4, +5 $M+H^+$ (M/z 569.7, 427.7, 342.3). Preparative purification was carried out on an Agilent 1100 HPLC with a Phenomenex Luna® 5 μm C18 100 Å LC Column 250 x 10 mm from 10-90% acetonitrile (Sigma) and water mixture with 0.01% TFA at a flow rate of 1.8 mL/min.

SNARF-4F was activated with ethyldicarbodiimide (Fluka Analytical) (1.0 eq.) and sulfosuccinimide sodium salt (Fluka Analytical) (5.0 eq.) in 100 mM 2-(*N*-

morpholino)ethanesulfonic acid (MES) buffer at pH 5.9. Reaction was monitored by Agilent 1100 HPLC/MS for completion over 2 hours with a Phenomenex Luna® 5 μm C18 100 Å LC Column 250 x 4.6 mm from 10-80% acetonitrile (Sigma) and water mixture with 0.01% TFA at a flow rate of 1.0 mL/min. The purified Ackxr$_9$ was added at 1.0 eq. to the solution and mixed overnight with a catalytic amount of dimethylaminopyridine. The labeled peptide was purified at 10-80% ACN/H_2O (0.01%) at a flow rate of 1.8 mL/min on a Phenomenex Luna® 5 μm C18 100 Å LC Column 250 x 10 mm and identified by +3, +4, +5 $M+H^+$ (M/z 799.7, 600.1, 480.3).

Cell Culture. HeLa cells were maintained in Dulbecco's Minimum Essential Medium (Life Technologies) supplemented with 10% fetal bovine serum and 1% penicillin/streptomycin. Cells were passaged when reaching 90% confluency. Cells were plated on #1 glass coverglass-bottom dishes 48 hours prior to imaging into 8-well Nunc Lab-Tek™ Chambered Coverglass (Thermo Scientific).

Transfection of Cells. Transfection solution was prepared with pCDNA3 vector containing CFP-4Cys (Appendix one) gene insert. Fugene HD (Roche) was used according to commercial protocol. Cells were transiently transfected 36-48 hours before imaging experiment.

Live cell epifluorescence imaging. FRET Imaging experiments to measure cytosolic delivery of r_9-FlAsH or r_9-FlAsH-r_9 was completed on an Axiovert 200M (Carl Zeiss Micro-Imaging, USA) inverted epifluorescence microscope with a Plan NeoFluar 40x oil

immersion objective (1.30 NA). CFP was imaged with a 420/20 bandpass excitation filter, 450 nm dichroic mirror, and 475/40 bandpass emission filter with 1 second exposure and 10% Neutral Density filter. All images were captured with a Photometrics Cascade II 1024 CCD camera (Photometrics, Tucson, AZ). Slidebook 4.0 by (Intelligent Imaging Innovations, Inc.) was used to capture and analyze images.

For standard imaging experiments, cells were imaged in 8-well chambers after being washed 3x with Hanks Buffered Saline Solution supplemented with 2g/L glucose at pH 7.4. CFP-4Cys transfected cells were imaged for up to 15 minutes prior to adding peptide-FlAsH. After the peptide is added in 10 min the well is washed and the peptide is applied again. This is necessary to maintain an accurate concentration of the peptide in solution due to peptide-FlAsH non-specifically binding to the plastic surfaces, depleting the soluble concentration (Appendix one).

Live cell confocal microscopy. HeLa cells were plated in a similar fashion to epifluorescence imaging experiments but remained untransfected. Cells were imaged using a Zeiss Observer.Z1 equipped with an LSM 5 Live confocal processor. SNARF-4F was excited with 532 nm laser and imaged with C-Apochromat UV-Vis-IR 40X water immersion lens. Fluorescence from the dye was collected with a 650 LP filter and 550-615 BP.

r_9-SNARF-4F in situ calibration. r_9-SNARF-4F was applied to HeLa cells at 2 μM concentration. Cells were given 25 minutes to endocytose the r_9-SNARF-4F. Internalized peptide and fluorophore were calibrated using the “null method” as

described by Eisner et al.[8] The pH was set at several points and the ratio of the two wavelengths emitted by SNARF-4F was measured from captured images from the confocal microscope. The measurements were then fit to a curve using Sigma Plot 10 (Systat Software, Inc., Point Richmond, CA). Measurements of endosomes were tracked and were extrapolated to the pH by the ratio measurements. (Appendix one)

Figures

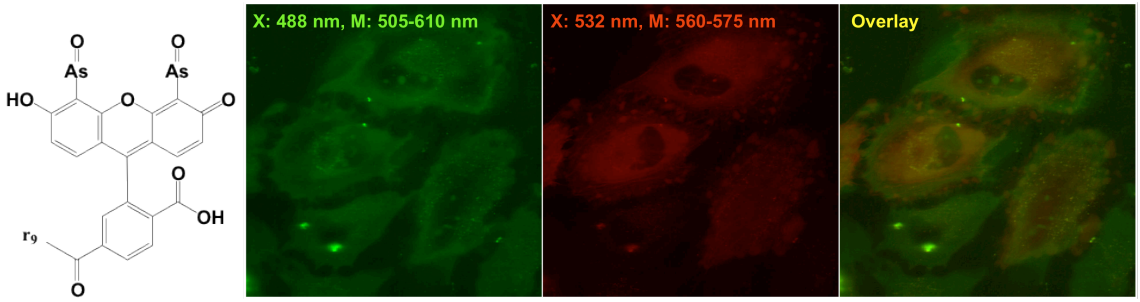

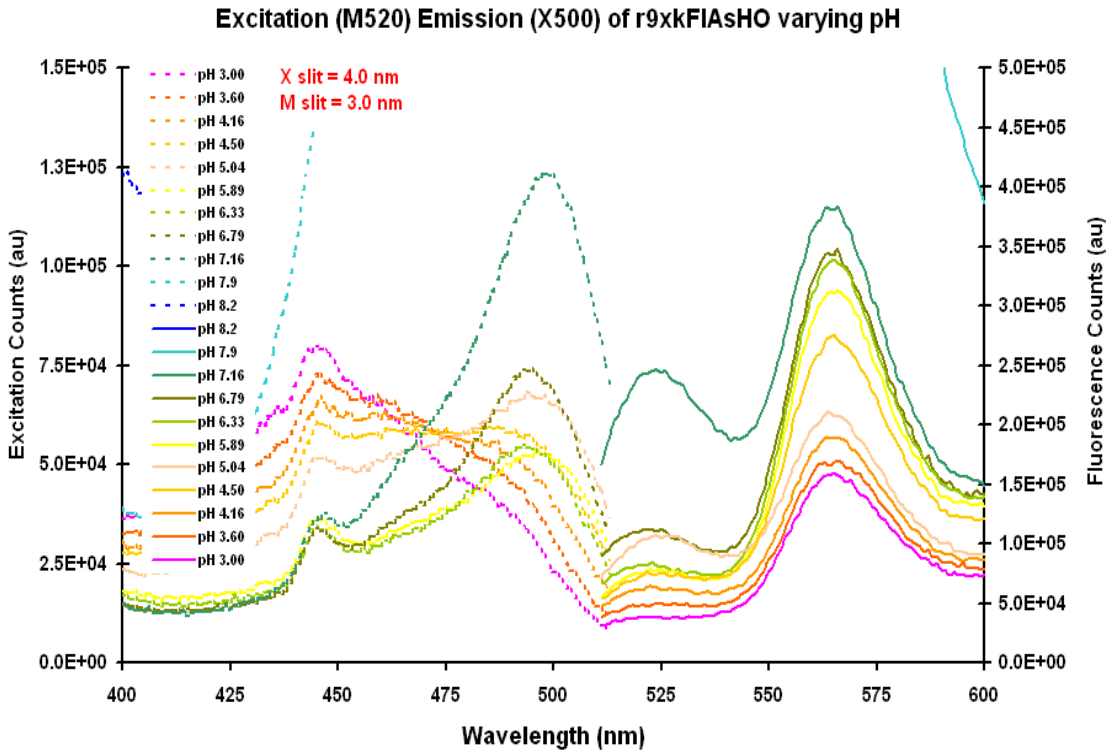

Figure 3.1 – *(above left)* FlAsH-O precursor to FlAsH. *(above right)* r_9-FlAsH-O imaged by confocal microscopy shows two species, one excited by 488 nm laser and one excited by 532 nm laser. *(below)* pH titration excitation and emission spectra of r_9-FlAsH-O.

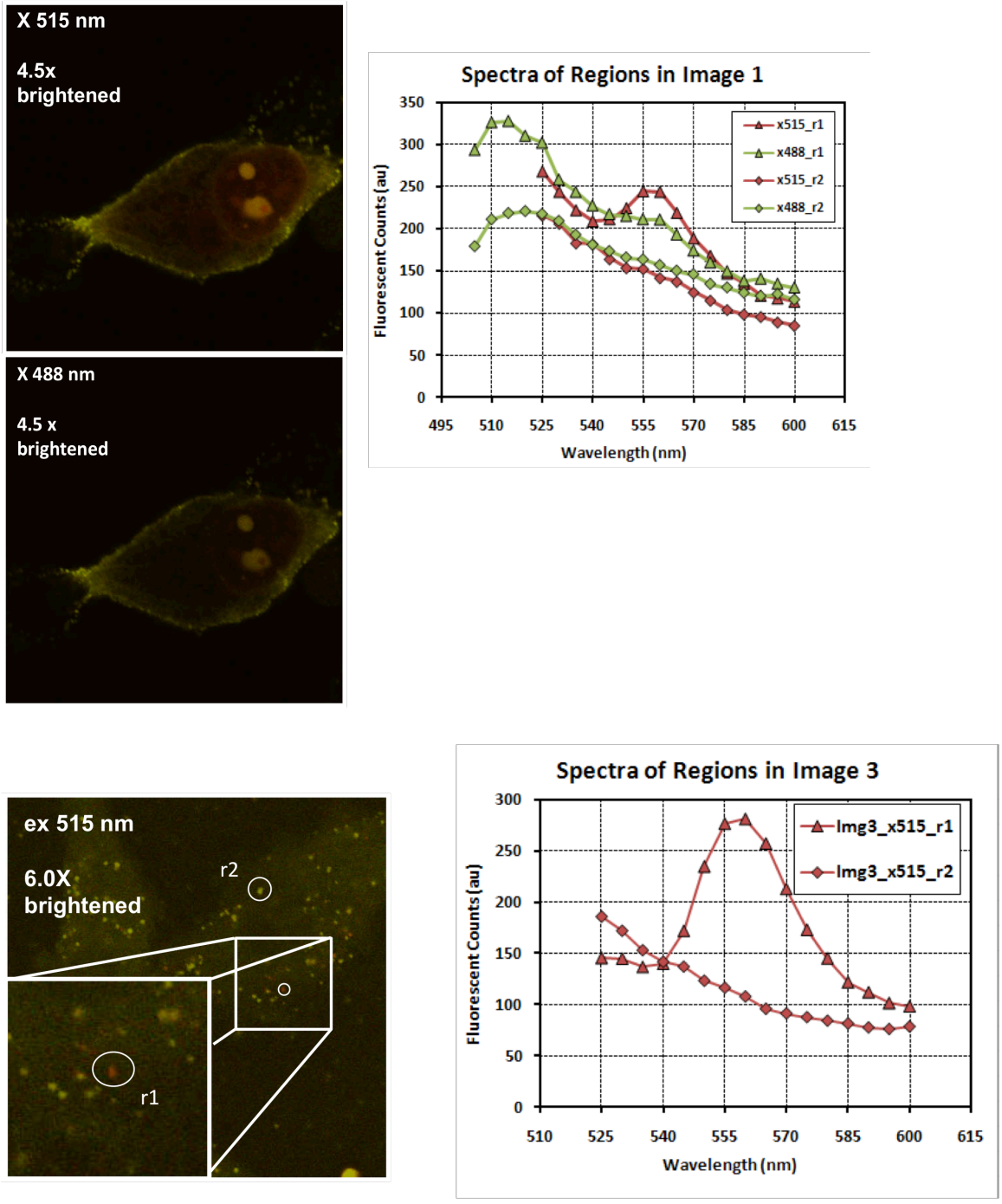

Figure 3.2 – r_9-FlAsH-O imaged by spectral imaging shows two separate species. *(above)*(r1) is within the nucleus, (r2) near the edge of the cell membrane. *(below)*

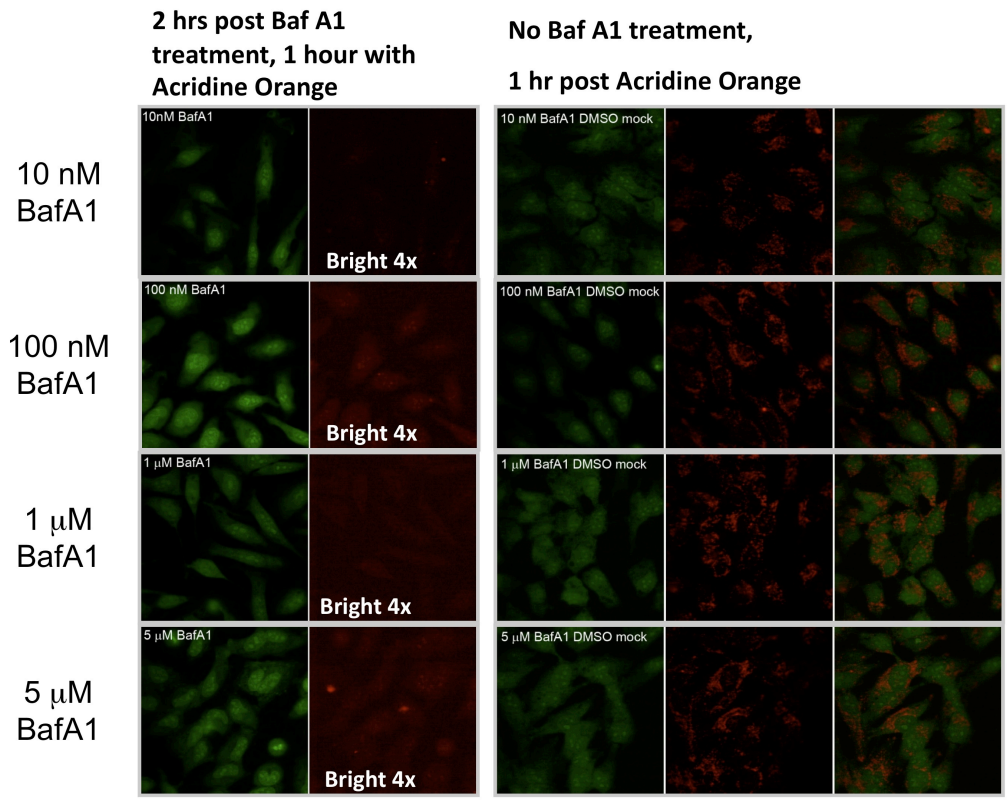

Figure 3.3 – Acridine orange accumulation in acidic vesicles/endosomes in HeLa cells is inhibited by Bafilomycin A1. Green is indicative of diffuse acridine orange dye and red is indicative of concentrated acridine orange inside acidic punctate vesicles, endosomes, and lysosomes.

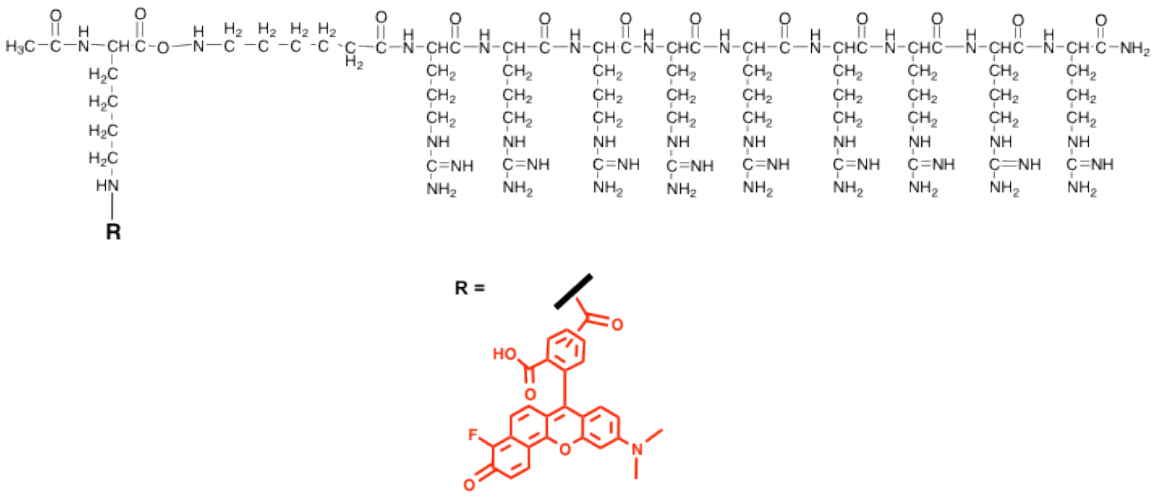

Figure 3.4 – r_9 peptide scaffold used for the study. SNARF-4F (5-,6-) carboxylic acid was attached via the ε-amine of D-Lysine.

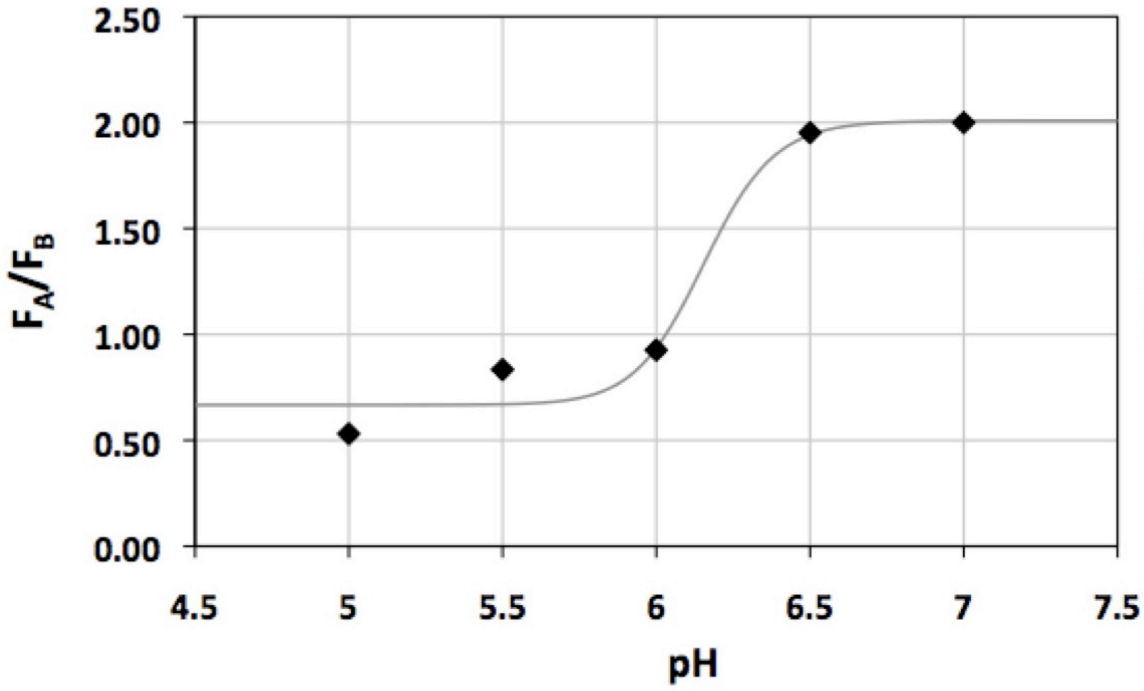

Figure 3.5 – *In situ* intracellular calibration of pH by SNARF-4F emission ratio response to pH changes as induced by "null method" for pH calibration.

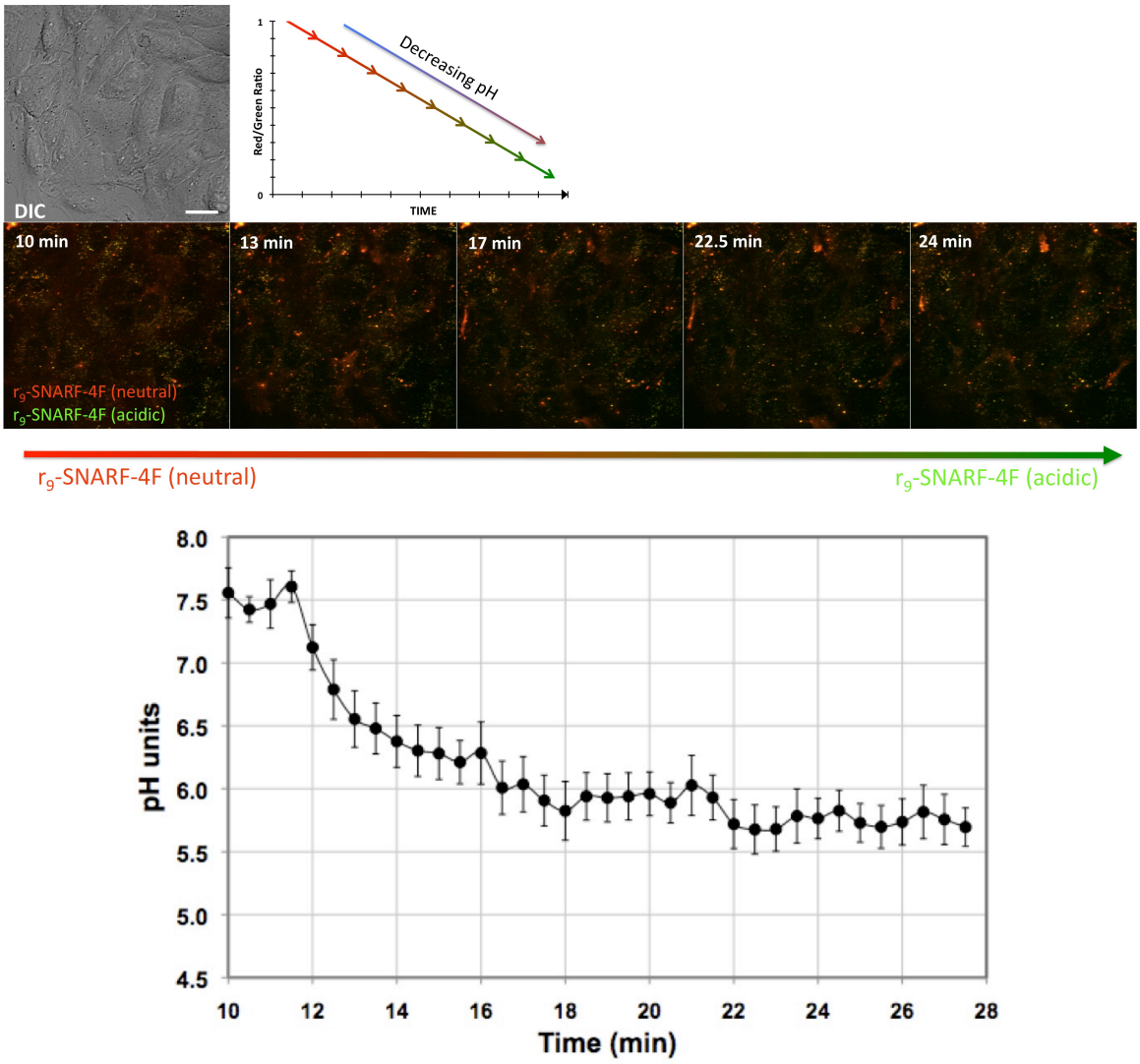

Figure 3.6 – r_9 peptide is endocytosed into endosome vesicles. *(above)* Maximum projection of HeLa cells taking up r_9-SNARF-4F over 25 minutes and indicates that the endosomes are initially neutral pH (red) and become acidified (green) over time. Scale bar is 10μm. *(below)* Time lapse pH measurement of endosomes containg r_9-SNARF-4F in HeLa cells (n = 8).

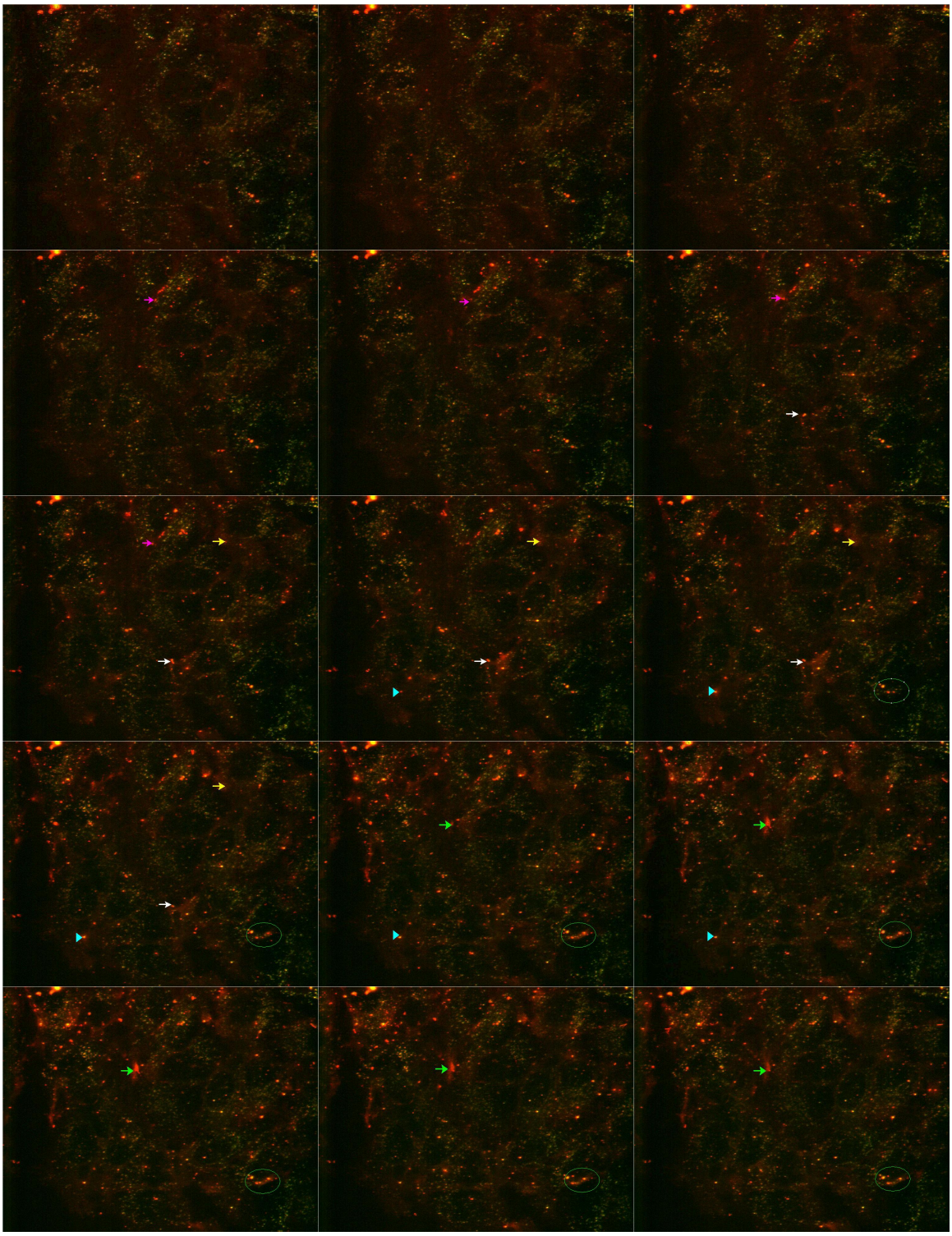

Figure 3.7 – Time lapse of r_9-SNARF-4F uptake into HeLa. Arrows and circled regions indicate several vesicle bursts of r_9-SNARF-4F released from endocytic vesicles. Frames spaced 30s apart viewed from top left to bottom right.

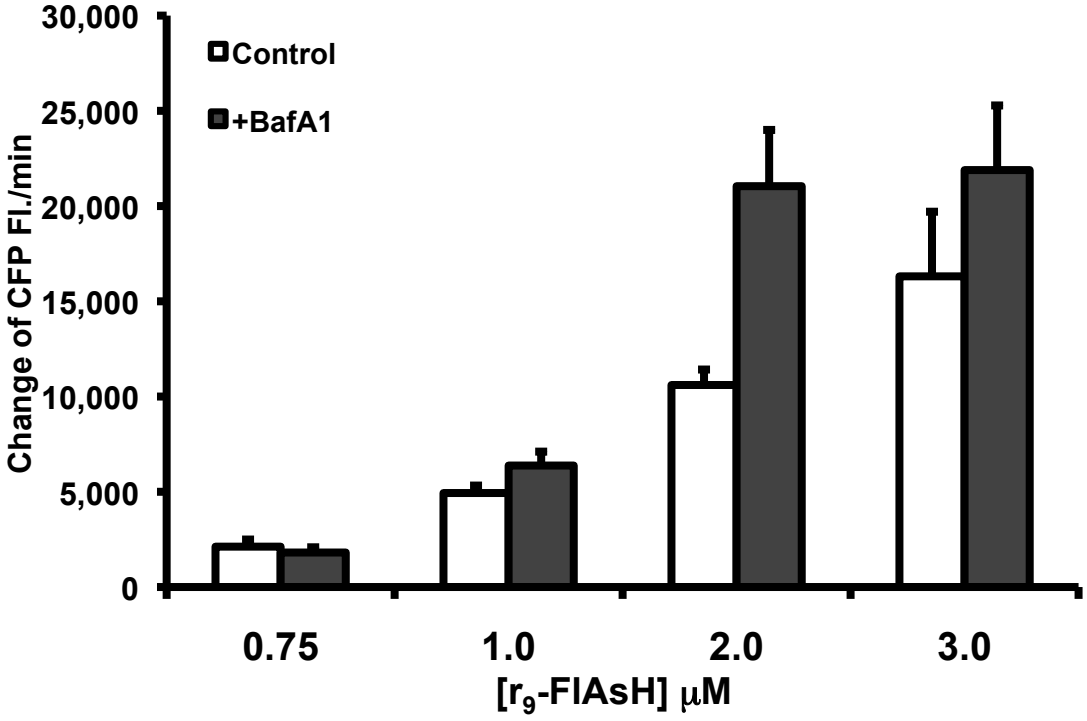

Figure 3.8 – Bafilomycin A1 (10 nM) affects the delivery rate of r_9-FlAsH.

Acknowledgement

Chapter three is currently being prepared for submission for publication. The dissertation author is the primary author. Co-authors include Dr. Stephen R. Adams, and Dr. Roger Y. Tsien. Additional thanks must be extended to Dr. Kaoru Saijo for reagents for pH sensor calibrations and Paul Steinbach for training and assistance with confocal imaging.

References

1. Fischer, R., Fotin-Mleczek, M., Hufnagel, H., and Brock, R. (2005) Break on through to the other side-biophysics and cell biology shed light on cell-penetrating peptides, *Chembiochem 6*, 2126–2142.

2. Nakase, I., Niwa, M., Takeuchi, T., Sonomura, K., Kawabata, N., Koike, Y., Takehashi, M., Tanaka, S., Ueda, K., and Simpson, J. (2004) Cellular uptake of arginine-rich peptides: roles for macropinocytosis and actin rearrangement, *Molecular therapy 10*, 1011–1022.

3. Wadia, J. S., Stan, R. V., and Dowdy, S. F. (2004) Transducible TAT-HA fusogenic peptide enhances escape of TAT-fusion proteins after lipid raft macropinocytosis, *Nat Med 10*, 310–315.

4. Mellman, I. (1992) The importance of being acid: the role of acidification in intracellular membrane traffic., *Journal of experimental biology 172*, 39 - 45.

5. Yoshimori, T., Yamamoto, A., Moriyama, Y., Futai, M., and Tashiro, Y. (1991) Bafilomycin A1, a specific inhibitor of vacuolar-type H (+)-ATPase, inhibits acidification and protein degradation in lysosomes of cultured cells., *J. Biol. Chem. 266*, 17707.

6. Geisow, M., Beaven, G., and Hart, P. (1980) Site of action of a polyanion inhibitor of phagosome-lysosome fusion in cultured macrophages, *Experimental Cell Research, 126*, 159-165.

7. "Lysosomes" The Cell: A Molecular Approach. 2nd edition. Cooper GM. Sunderland (MA): Sinauer Associates; 2000.

8. Eisner, D., Kenning, N., O'Neill, S., Pocock, G., Richards, C., and Valdeolmillos, M. (1989) A novel method for absolute calibration of intracellular pH indicators, *Pflügers Archiv European Journal of Physiology 413*, 553–558.

9. Duchardt, F., Mleczek, M. F., and Schwarz, H. (2007) A Comprehensive Model for the Cellular Uptake of Cationic Cell-penetrating Peptides. *Traffic 8,* 848–866.

Chapter Four

Comparison of localization and delivery efficiency of r_9 and non-peptide guanidinium-rich molecular transporters

Abstract

The guanidinium groups of arginine amino acids mediate the interaction of cell penetrating peptides with heparin sulfate proteoglycans on the surface of cells. Guanidinoneomycin and D-Arg9 were synthesized and studied to discern their ability to localize in the cytosol of live cells. A cell-based FRET assay was used to extrapolate kinetic data and quantify the molecules in the cytosol. The data demonstrate that although these two transporters maintain similar overall cellular uptake, the rate at which they release into the cytosol is quite distinct. Furthermore, we are able to quantify the transporter delivered specifically to the cytosol.

Introduction

Since the discovery that guanidinylation can lead to increased cellular uptake, numerous guanidinium based molecular transporters (GRTs) have been developed on an array of scaffolds.[1-4] While initial attempts in the field were aimed at deciphering a single model of internalization and shared delivery properties, it is growing increasingly clear that each class of transporters maintains its own distinct delivery profile.[5] Typically, studies revolve around overall cellular uptake as determined by flow cytometry, or intracellular delivery monitored by microscopy.[6] However, it is difficult to visualize and characterize the uptake pathway or kinetic data of cytosolic delivery in live cells. Transporter localization and kinetic information is crucial for the growing effort to utilize these types of molecules as therapeutic delivery agents, as most intracellular therapeutics require cytosolic delivery.[7,8]

Literature data suggest that while GRTs can deliver cargo to the cytosol, although the specific mechanism by which this process occurs is unknown,[9] endosomal trapping is a primary issue preventing these molecules from being useful for therapeutic drug delivery.[8] Additionally, it is unclear how much and at what rate the cargo reaches its targeted destination.[10,11] While current methods exist to evaluate this information, they suffer from a lack of sensitivity or an inability to observe data in real time.[12-15] In this report, we analyze and quantify the rate of cytosolic-delivery of these two transporters, using confocal microscopy and a cell-based FRET assay. Specifically, D-Arg_9 (r_9) and guanidinoneomycin (Gneo, Figure 4.1) are investigated for their ability to present into the cytosol.

Results and Discussion

Utilizing orthogonal dyes, confocal microscopy studies were performed using TAMRA-Gneo and Cy5-r_9 (Figure 4.2) to determine their independent and combined distribution inside live cells. In agreement with previous reports, puncta formation is largely prevalent for both transporters. The guanidinoneomycin-TAMRA conjugate displays significantly more punctate localization than its r_9-Cy5 counterpart at similar concentrations. Interestingly, the transporters appear to co-localize. Based on these images, however, it is difficult to discern how much of the transporters are present in the cytosol.

To expand our ability to characterize intracellular events, a cell-based FRET assay described by Tsien and co-workers was used to determine and quantify the rate at which

the transporters localize into the cytosol.[16,17] The assay utilizes bi-arsenical fluorescein (FlAsH)-labeled conjugates that, only upon internalization and exposure to the cytosol, bind to the tetracysteine tag expressed on cyan-fluorescent protein (CFP-4Cys).[18-21] FlAsH conjugates binding to CFP-4Cys results in the formation of a reportable FRET pair, where CFP acts as the FRET donor and FlAsH as the FRET acceptor.[18] By monitoring the rate at which the fluorescence changes over time, kinetic information can be extrapolated and quantified in live cells.[22] The assay, however, cannot take into account which pathway the transporters use to gain entry to the cell and eventually present in the cytosol.

FlAsH-labeled conjugates of Gneo and r_9 were synthesized and exposed to CFP-4Cys-transfected HeLa cells.[16,20,23] The initial rates, in pM/min, were obtained and plotted in Figure 4.3.[23,24] The r_9 conjugate demonstrates a 2–4 fold improved rate of cytosolic delivery compared to Gneo. It is worth noting that at concentrations of 5μM and above the r_9 conjugates were found to be cytotoxic, whereas the Gneo conjugates were not.[8,25] The cytosolic rate of r_9 uptake appears to attenuate and become constant, this is perhaps due to a maximum rate of endocytosis or transporter release. Gneo, however, continues to increase linearly in this range.

The data suggests that while both transporters internalize similarly, their rate of release into the cytosol is quite distinct. Indeed, it appears that Gneo suffers from endosomal trapping more than r_9. The tendency of Gneo to be trapped is reported and hypothesized to be a result of its selective affinity toward heparan sulfate glycosaminoglycans.[26,27] Arginine-rich transporters, however, do not share this selectivity.[25]

Conclusion

Overall, the data support the trend that various guanidinylated scaffolds have distinct, but not entirely unique, delivery profiles. While r_9 displays superior cytosolic delivery to guanidinoneomycin, it can alternatively be stated that guanidinoneomycin is a superior vector for delivery to endosomal/lysosomal vesicles. This technique has already been utilized for therapeutic treatment of lysosomal storage diseases.[27]

Materials and Methods

Peptide synthesis, purification, validation, and fluorophor labeling. Peptide was prepared by standard solid phase Fmoc (9-fluorenylmethyloxycarbonyl) synthesis methods with NovaSyn® TGR resin. Prior to cleavage the peptide was capped by an acetyl group on the amino termini with 66% acetic anhydride (Sigma), 17% Lutidine base (Sigma), 17% acetic anhydride (Sigma), and a catalytic quantity of dimethyl-amino-pyridine (Sigma) at 5x volume of the resin, mixed for 2 hours at room temperature. The peptide is cleaved from the resin by an acidic solution composed of 94% trifluoroacetic acid (TFA, Acros Organics), 2% triisopropylsilane (Sigma), 2% ethanedithiol (Fluka Analytical), and 2% thioanisole (Sigma) and mixed for 2 hours at room temperature to cleave. Upon cleavage the carboxyl termini attached to the resin is converted to an amide. The peptide was composed of acetylated D-lysine, aminohexanoic acid (x), and nine D-arginines ($Ackxr_9$). Once cleaved the peptide was analyzed on an Agilent 1100 HPLC/MS with a Phenomenex Luna® 5 μm C18 100 Å LC Column 250 x 4.6 mm from 10-90% acetonitrile (Sigma) and water mixture with 0.01% TFA at a flow rate of 1.0 mL/min and the peptide mass identified in the positive ion mode at the +3, +4, +5 $M+H^+$ (M/z 569.7, 427.7, 342.3). Preparative purification was carried out on an Agilent 1100 HPLC with a Phenomenex Luna® 5 μm C18 100 Å LC Column 250 x 10 mm from 10-90% acetonitrile (Sigma) and water mixture with 0.01% TFA at a flow rate of 1.8 mL/min.

UV-Vis. Concentrations for FlAsH and Cy5 labeled compound solutions were determined using Nano Drop 2000C and literature values for extinction coefficients.

Flow Cytometry. 75000 HeLa cells were counted by using a hemocytometer, transferred to 48-well plates, and incubated in DMEM (300 μL of media; with a 1% solution of penicillin/streptomycin and 10% FBS) overnight at 37°C. The cells were then washed with PBS and treated with a solution of the corresponding compound (75 μL; DMEM containing 10% FBS) and incubated. Following this, the cells were washed twice with PBS to remove any remaining extracellular compound. The cells were then detached with trypsin/EDTA (50 μL), diluted with medium (50 μL) and FACS buffer (50 μL), and analyzed by flow cytometry. Cellular uptake was quantified by the mean fluorescence intensity; the crude data were interpreted by using FlowJo v8.8.6 wherein the median value was determined and later plotted and further analyzed by using OriginPro 8.

Preparation of r_9-Cy5. Cy5-NHS, 4-dimethylaminopyridine, and *N*,*N*-diisopropylethylamine were added to r_9 in DMF for 12 h at RT. The crude product was purified on a C-18 reverse phase HPLC column using a gradient of 10–90% acetonitrile (0.1% TFA) in water (0.1% TFA) over 20 minutes (3mL/min). The compound eluted as a TFA salt at 6.2 min. HR-ESI-FT-MS calculated for $C_{101}H_{178}N_{42}O_{19}S_2$ $[M+4H]^{+4}$ 586.8418 and found 586.8416.

Preparation of r_9-FlAsH. Succinylated-carboxy-FlAsH$(EDT)_2$ obtained from Dr. Stephen Adams, was mixed with 1.5 eq. purified Ackxr_9 or Ac$r_9$xkxr_9 in DMSO with 1.0

eq. diisopropylethylamine (Aldrich) and monitored overnight by Agilent 1100 HPLC/MS for completion. The labeled peptide was purified at 10-90% ACN/H_2O (0.01%) at a flow rate of 1.8 mL/min on a Phenomenex Luna® 5 μm C18 100 Å LC Column 250 x 10 mm and identified by HR-ESI-TOFMS calculated for $C_{93}H_{155}As_2N_{40}O_{23}S_2$ $[M+3H]^{+3}$ 799.3247 and found 799.3235.

Cell Culture. HeLa cells were maintained in Dulbecco's Minimum Essential Medium (Life Technologies) supplemented with 10% fetal bovine serum and 1% penicillin/streptomycin. Cells were passaged when reaching 90% confluency. Cells were plated on #1 glass coverglass-bottom dishes 48 hours prior to imaging into 8-well Nunc Lab-Tek™ Chambered Coverglass (Thermo Scientific).

Transfection of Cells. Transfection solution was prepared with pCDNA3 vector containing CFP-4Cys (Appendix 1) gene insert. Fugene HD (Roche) was used according to commercial protocol. Cells were transiently transfected 36-48 hours before imaging experiment.

Live cell epifluorescence imaging. FRET Imaging experiments to measure cytosolic delivery of r_9-FlAsH or r_9-FlAsH-r_9 was completed on an Axiovert 200M (Carl Zeiss Micro-Imaging, USA) inverted epifluorescence microscope with a Plan NeoFluar 40x oil immersion objective (1.30 NA). CFP was imaged with a 420/20 bandpass excitation filter, 450 nm dichroic mirror, and 475/40 bandpass emission filter with 1 second exposure and 10% Neutral Density filter. All images were captured with a Photometrics

Cascade II 1024 CCD camera (Photometrics, Tucson, AZ). Slidebook 4.0 by (Intelligent Imaging Innovations, Inc.) was used to capture and analyze images.

During imaging experiments, cells were imaged in 8-well chambers after being washed 3x with Hanks Buffered Saline Solution supplemented with 2g/L glucose at pH 7.4. CFP-4Cys transfected cells were imaged for up to 15 minutes prior to adding peptide-FlAsH. After the peptide is added in 10 min the well is washed and the peptide is applied again. This is due to peptide-FlAsH non-specifically binding to the plastic surfaces as measured by absorbance (Fig. A1.2-A1.4).

Figures

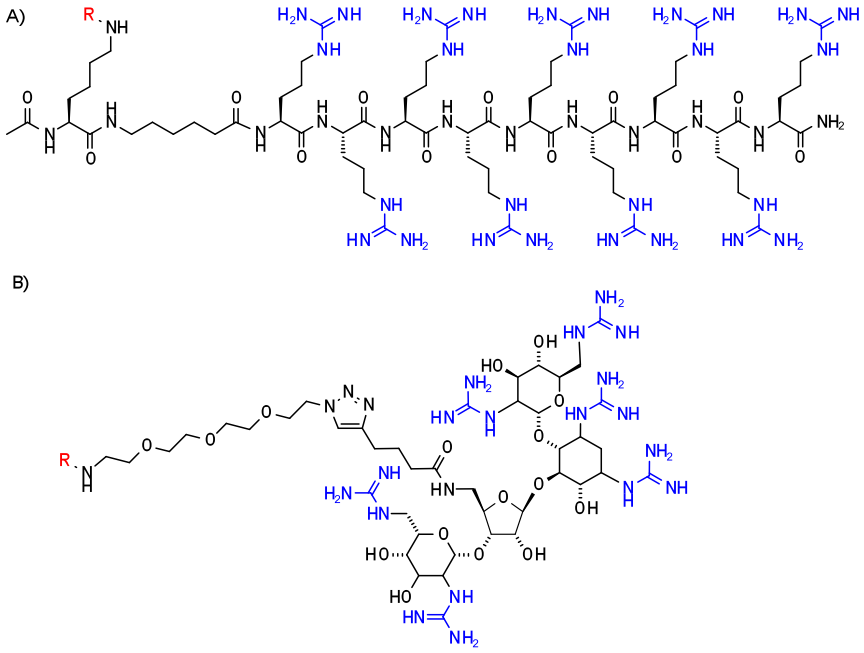

Figure 4.1 – Structures of A) r_9 , and B) guanidinoneomycin. R = Cy5, FlAsH, or TAMRA. Guanidine groups are highlighted in blue.

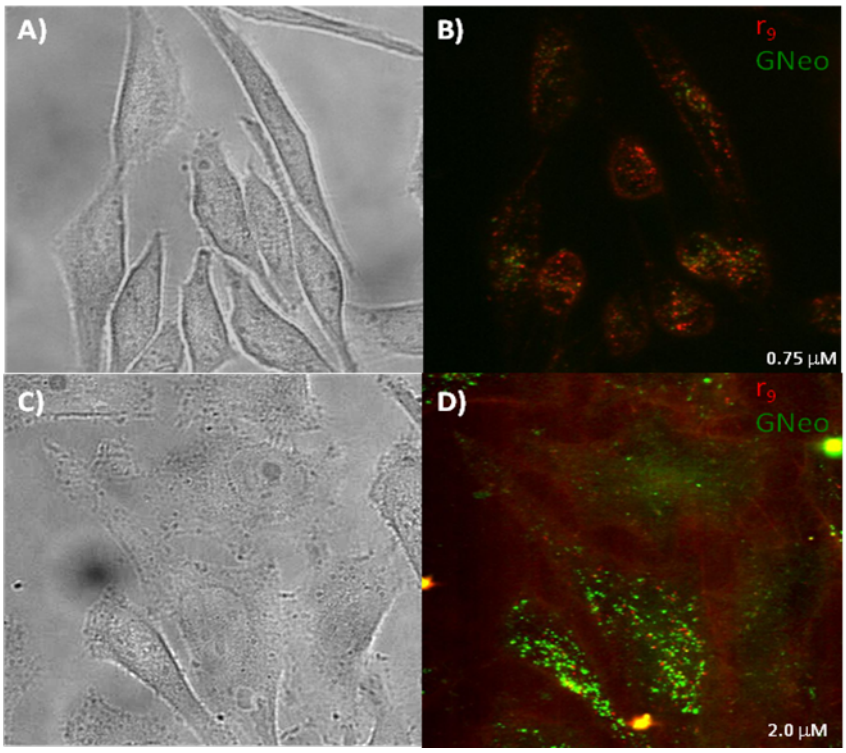

Figure 4.2 – Confocal microscopy images highlighting co-localization and internalization of guanidinoneomycin-TAMRA and Arg_9-Cy5. A) DIC image, B) 0.75 μM transporters, C) DIC image, D) 2.0 μM transporters. Images are taken after 60 minutes.

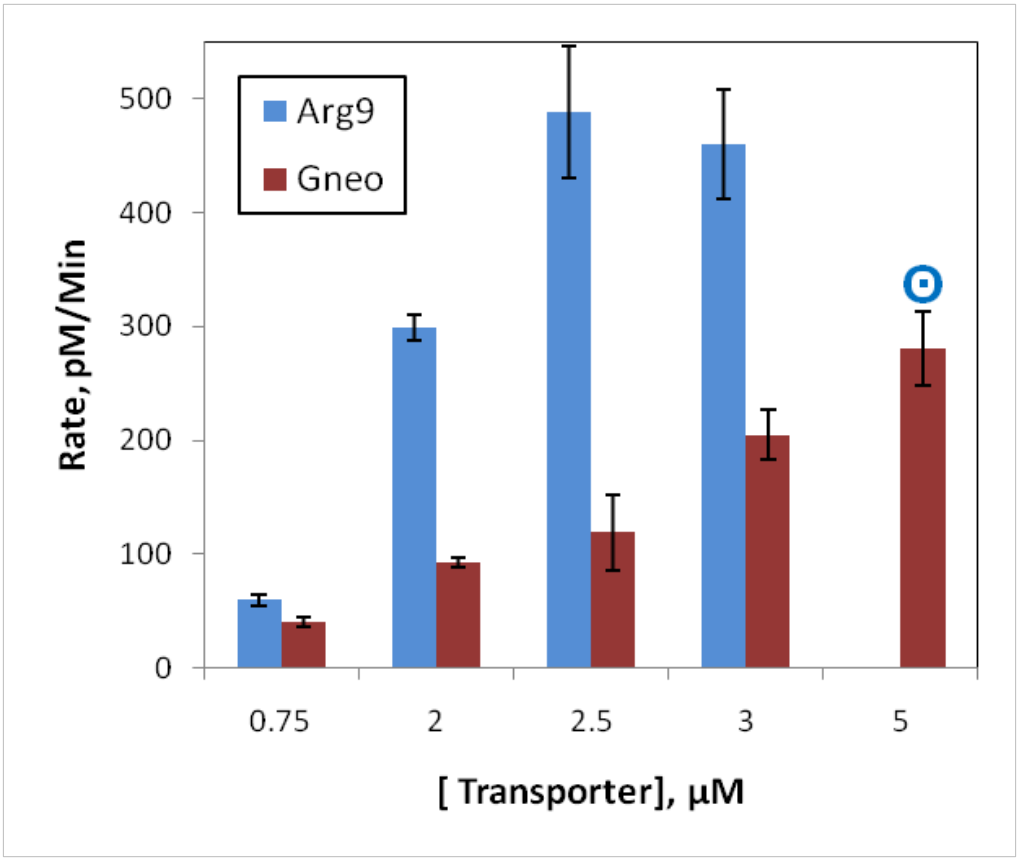

Figure 4.3 – Comparison of the rate of endosomal escape. Key: r_9 ■, and gneo ■. Note that r_9 was toxic at 5μM (⊙).

Acknowledgement

Chapter four is currently being prepared for submission for publication. The dissertation author was a primary author. Co-authors include Dr. Andrew Dix, Dr. Yitzhak Tor, and Dr. Roger Y. Tsien.

References

1. Rothbard, J. B.; Jessop, T. C.; Wender, P. A. (2005) *Adv Drug Deliver Rev*, *57*, 495–504.

2. Futaki, S. (2005) *Adv Drug Deliver Rev*, *57*, 547–558.

3. Wadia, J. S.; Dowdy, S. F. (2003) *Curr Protein Pept Sc*, *4*, 97–104.

4. Futaki, S.; Goto, S.; Sugiura, Y. (2003) *Journal of Molecular Recognition* , *16*, 260–264.

5. Wender, P. A.; Galliher, W. C.; Goun, E. A.; Jones, L. R.; Pillow, T. H. (2008) *Adv Drug Deliver Rev* , *60*, 452–472.

6. Chung, S. K.; Maiti, K. K.; Lee, W. S. (2008) *Int J Pharm* , *354*, 16–22.

7. Wright, L. R.; Rothbard, J. B.; Wender, P. A. (2003) *Curr Protein Pept Sc* , *4*, 105–124.

8. Temsamani, J.; Vidal, P. (2004) *Research Focus* , *9*, 1012–1019.

9. Futaki, S. (2006) *Biopolymers* , *84*, 241–249.

10. Richard, J. P.; Melikov, K.; Vives, E.; Ramos, C.; Verbeure, B.; Gait, M. J.; Chernomordik, L. V.; Lebleu, B. (2003) *J Biol Chem* , *278*, 585–590.

11. Ziegler, A.; Nervi, P.; Durrenberger, M.; Seelig, J. (2005) *Biochemistry–Us* , *44*, 138–148.

12. Hallbrink, M.; Floren, A.; Elmquist, A.; Pooga, M.; Bartfai, T.; Langel, U. (2001) *Biochim Biophys Acta* , *1515*, 101–109.

13. Saito, G.; Swanson, J. A.; Lee, K. D. *Adv Drug Deliv Rev* 2003, *55*, 199–215.

14. Soughayer, J. S.; Wang, Y.; Li, H.; Cheung, S. H.; Rossi, F. M.; Stanbridge, E. J.; Sims, C. E.; Allbritton, N. L. (2001) *Biochemistry–Us* 2004, *43*, 8528–8540.

15. Zaro, J. L.; Shen, W. C. (2001) *Biochem Biophys Res Commun* 2003, *307*, 241–247.

16. Adams, S. R.; Tsien, R. Y.; 2nd ed.; Langel, U., Ed. 2006.

17. Adams, S. R.; Tsien, R. Y. (2008) *Nat Protoc*, *3*, 1527–1534.

18. Griffin, B. A.; Adams, S. R.; Tsien, R. Y. (1998) *Science* , *281*, 269–272.

19. Griffin, B. A.; Adams, S. R.; Jones, J.; Tsien, R. Y. (2000) *Methods Enzymol*, *327*, 565–578.

20. Adams, S. R.; Campell, R. E.; Gross, L. A.; Martin, B. R.; Walkup, G. K.; Yao, Y.; Llopis, J.; Tsien, R. Y. (2002) *J. Am. Chem Soc*, *124*, 6063–6076.

21. Gaietta, G.; Deerinck, T.; Adams, S. R.; Bouwer, J.; Tour, J.; Laird, D. W.; Sosinsky, G. E.; Tsien, R. Y.; Ellisman, M. (2002) *Science* , *296*, 503–507.

22. FlAsH binds to the tetra–cysteine label of CFP in a stochiometric fashion causing a decrease in the flourescence emission of CFP. This change can be monitored over time to give kinetic information. See Chapter two

23. See Chapter two.

24. Calibration was done using a series of known CFP concentrations. See Chapter two.

25. Elson-Schwab, L.; Garner, O. B.; Schuksz, M.; Crawford, B. E.; Esko, J. D.; Tor, Y. (2007) *J Biol Chem* , *282*, 13585–13591.

26. Dix, A. V.; Fischer, L.; Sarrazin, S.; Redgate, C. P. H.; Esko, J. D.; Tor, Y. (2010) *Chembiochem* , *11*, 2302–2310.

27. Sarrazin, S.; Wilson, B.; Sly, W. S.; Tor, Y.; Esko, J. D. (2010) *Nature Molecular Therapy* , *18*, 1268–1274.

Chapter Five

Studies of the affects of pharmacological agents on the cytosolic delivery of r_9-FlAsH

Abstract

Many proteins govern the endocytosis machinery. Each protein function independently, but interact to control critical steps of the machinery without which the mechanism would be incapacitated. Biochemists have used various pharmacological inhibitors to attempt to elucidate the steps of the endocytosis mechanism. In the field of CPP, biochemists have equally employed pharmacological agents to attempt to undestand the mechanisms that enable the entry of these peptides into a cell. Here we present a study of three pharmacological agents that are inhibitors or agonists of proteins implicated in the critical steps of endocytosis of CPPs. Using wortmannin, PMA and chloroquine, we explore how the effects of these molecules on the cell affect the cytosolic release of r_9 CPP.

Introduction

Since a clear consensus established that cell penetrating peptides (CPPs) are internalized by various endocytic processes the various endocytic routes have been probed through pharmacological agents that perturb the endocytic mechanisms. The various endocytic mechanisms are a result of coordination of many hundreds of proteins. Some proteins have equivalent roles in endocytosis like actin or microtubules, but others only play specific roles in trafficking or maturation of vesicles.[1-3]

In the endocytic mechanism the internalization process is dependent on cytoskeletal components but also sorting proteins. Cytoskeletal components like actin and microtubules create the tracks and motion of the endocytosed vesicles throughout the

cells, while other proteins ensure that vesicles continuously move through the process of degradation or trafficking to the correct organelle. Two proteins that play a main role in the trafficking process are phosphatidyl-inositol-3-OH kinase (PI(3)K) and protein kinase C (PKC). Both are implicated in steps of the endocytic processes that also internalize CPPs.[2]

PI(3)K is implicated in several points of the trafficking of endosomes. PI(3)K may be involved with the fusing of early endosomes with late endosomes as well as in the cycling of receptors to the surface of cells.[4,5] By using an inhibitor for PI(3)K, wortmannin (Fig. 5.1), in a model of CPPs of arginine$_8$ (R_8) Nakase et al. concluded that a reduction of delivery of the peptide by indirect measurement of reduced cell death as compared to a control. In contrast to Nakase et al. Duchardt et al. notes that wortmannin had no effect on the internalization of R_9 peptides.[4,6]

PKC plays various roles in cell growth and proliferation. With respect to CPP endocytosis, PKC is an activator of macropinocytosis, which is the implicated endocytic pathway for polyarginine endocytosis.[7,8] There is some evidence to indicate that phorbol (phorbol 12-myristate 13-acetate, PMA, Fig. 5.1) stimulation of PKC can enhance the fusion of endosomes as well.[9]

Within the scope of pharmacological agents that can be tested a question remains as to the efficiency of some supposed endosome breaking agents, or lysosomotropic agents. Chloroquine is a common lysosomotropic agent used to investigate peptide release into the cytoplasm (Fig. 5.1). Chloroquine can perturb vesicles by either slowing acidification or by accumulating counterions in the endosome and eventually causing the breakage and release of the vesicle contents.

Using a measure of D-arginine$_9$ (r_9) entry into endosomes (see Chapter two), we investigate the affect of PMA, wortmannin, and chloroquine on the rate of r_9 release into the cytosol and nucleus. PMA enhanced the rate of delivery slightly of r_9, while wortmannin had no significant measureable effect on the delivery rate of r_9. Chloroquine did indicate an increased rate of delivery of r_9.

Results and Discussion

The delivery efficiency and delivery rate of r_9 is an important aspect of the utility of this molecule to be useful as a drug delivery molecule. In order to better understand how this molecule may be useful the mechanism by which it is taken into cell is a critical characteristic to elucidate. In hopes of learning more about the mechanism of uptake and the affect on the efficiency of the delivery rate of r_9 to the cytosol, PMA, wortmannin and chloroquine were used to perturb proteins or the biochemistry of the endocytic mechanism.

PMA stimulation results in an average increase in the rate of r_9-FlAsH cytosolic delivery. PMA was expected to stimulate membrane ruffling which can also enhance the level of endocytosis. PMA is also implicated to enhance vesicle fusion after endocytosis. Stimulation of membrane ruffling was expected to enhance peptide uptake and thus increase the probability of release from endosomes, whereas it was not clear that vesicle fusion should enhance endosomal release or uptake.

PMA use in CFP-4Cys transfected HeLa cells enhances the delivery rate of r_9-FlAsH (Figure 5.2). The enhancement by PMA did not pass the student's t-test for

significance, but there is an average increase in the uptake that could be a result of the increased ruffling. The rate of delivery in presence of PMA was increased slightly as the concentration increased over the range of concentrations from 0.75μM – 2μM. Stimulation by PMA is not enough to increase uptake of the low extracellular peptide concentrations compared to the rate of uptake of high extracellular concentrations of peptide in control samples.

Wortmannin does not significantly inhibit or enhance the delivery rate of r_9-FlAsH. Vesicle cycling and trafficking is affected by PI(3)K. Wortmannin (WM) can block the cycling of vesicles and may provide more time in the early endosome state preventing fusion to late endosomes. Figures 5.3 presents data which indicates no statistically significant effect on the rate of r_9-FlAsH delivery. On average the highest improvement in the delivery rate is at 3μM. This conservative improvement of r_9-FlasH delivery may be attributed to the prevention of vesicle cycling and fusion, providing slightly more time to enhance r_9-FlAsH release. At all other tested concentrations WM had little or no significant effect on the delivery rate of r_9-FlAsH.

Chloroquine enhances endosomal sequestered r_9-FlAsH delivery. Endosomal escape is the limiting step of r_9-FlAsH delivery. To enhance delivery lysosomotropic agents are expected to be a very useful. Chloroquine (CQ) is commonly used to show that CPPs are sequestered predominantly in endosomes. Although CQ is the standard method of breaking endosomes it is very dependent on acidity of vesicles containing CPPs in order to break endosomes. It is not clear that all CPPs follow the same endocytic route thus all peptides may not be endocytosed into vesicles that become acidic. To gain a better

understanding of the role of CQ with respect to r_9, r_9-FlAsH delivery was tested in presence of CQ.

In presence of CQ r_9-FlAsH delivery rate was enhanced minimally at 0.75 μM r_9-FlAsH application (Figure 5.4). As r_9-FlAsH concentration increased to 1μM and higher, CQ appeared to have an increased affect (2.5x) on the delivery rate. Thus, the indication was that CQ may be breaking the endosomes inside which r_9 is sequestered. The affect of CQ does appear to taper off at 3μM, but this was the highest concentration tested in this assay. The data confirm that CQ enhances cytoslic release of r_9-FlAsH but not to the extent that has been reported previously.

Materials and Methods

Peptide synthesis, purification, validation, and fluorophor labeling. Peptide was prepared by standard solid phase Fmoc (9-fluorenylmethyloxycarbonyl) synthesis methods with NovaSyn® TGR resin. Prior to cleavage the peptide was capped by an acetyl group on the amino termini with 66% acetic anhydride (Sigma), 17% Lutidine base (Sigma), 17% acetic anhydride (Sigma), and a catalytic quantity of dimethyl-amino-pyridine (Sigma) at 5x volume of the resin, mixed for 2 hours at room temperature. The peptide is cleaved from the resin by an acidic solution composed of 94% trifluoroacetic acid (TFA, Acros Organics), 2% triisopropylsilane (Sigma), 2% ethanedithiol (Fluka Analytical), and 2% thioanisole (Sigma) and mixed for 2 hours at room temperature to cleave. Upon cleavage the carboxyl termini attached to the resin is converted to an amide. The peptide was composed of acetylated D-lysine, aminohexanoic acid (x), and

nine D-arginines (Ackxr$_9$). Once cleaved the peptide was analyzed on an Agilent 1100 HPLC/MS with a Phenomenex Luna® 5 μm C18 100 Å LC Column 250 x 4.6 mm from 10-90% acetonitrile (Sigma) and water mixture with 0.01% TFA at a flow rate of 1.0 mL/min and the peptide mass identified in the positive ion mode at the +3, +4, +5 M+H$^+$ (M/z 569.7, 427.7, 342.3). Preparative purification was carried out on an Agilent 1100 HPLC with a Phenomenex Luna® 5 μm C18 100 Å LC Column 250 x 10 mm from 10-90% acetonitrile (Sigma) and water mixture with 0.01% TFA at a flow rate of 1.8 mL/min.

Cell Culture. HeLa cells were maintained in Dulbecco's Minimum Essential Medium (Life Technologies) supplemented with 10% fetal bovine serum and 1% penicillin/streptomycin. Cells were passaged when reaching 90% confluency. Cells were plated on #1 glass coverglass-bottom dishes 48 hours prior to imaging into 8-well Nunc Lab-Tek™ Chambered Coverglass (Thermo Scientific).

Transfection of Cells. Transfection solution was prepared with pCDNA3 vector containing CFP-4Cys (Appendix 1) gene insert. Fugene HD (Roche) was used according to commercial protocol. Cells were transiently transfected 36-48 hours before imaging experiment.

Live cell epifluorescence imaging. FRET Imaging experiments to measure cytosolic delivery of r$_9$-FlAsH or r$_9$-FlAsH-r$_9$ was completed on an Axiovert 200M (Carl Zeiss Micro-Imaging, USA) inverted epifluorescence microscope with a Plan NeoFluar 40x oil

immersion objective (1.30 NA). CFP was imaged with a 420/20 bandpass excitation filter, 450 nm dichroic mirror, and 475/40 bandpass emission filter with 1 second exposure and 10% Neutral Density filter. All images were captured with a Photometrics Cascade II 1024 CCD camera (Photometrics, Tucson, AZ). Slidebook 4.0 by (Intelligent Imaging Innovations, Inc.) was used to capture and analyze images.

For standard imaging experiments, cells were imaged in 8-well chambers after being washed 3x with Hanks Buffered Saline Solution supplemented with 2g/L glucose at pH 7.4. CFP-4Cys transfected cells were imaged for up to 15 minutes prior to adding peptide-FlAsH. After the peptide is added in 10 min the well is washed and the peptide is applied again. This is necessary to maintain an accurate concentration of the peptide in solution due to peptide-FlAsH non-specifically binding to the plastic surfaces, depleting the soluble concentration (Appendix 1). Wortmannin was to a final concentration of 75 nM added 30 minutes prior to imaging and imaging was continued as normal. PMA was added with r_9-FlAsH concentrations at 2.5 μM. Chloroquine was added 20 minutes before the experiment was started at 75 μM. All concentrations of pharmacological agents were added at the same concentration to the bath at refresh step.

Figures

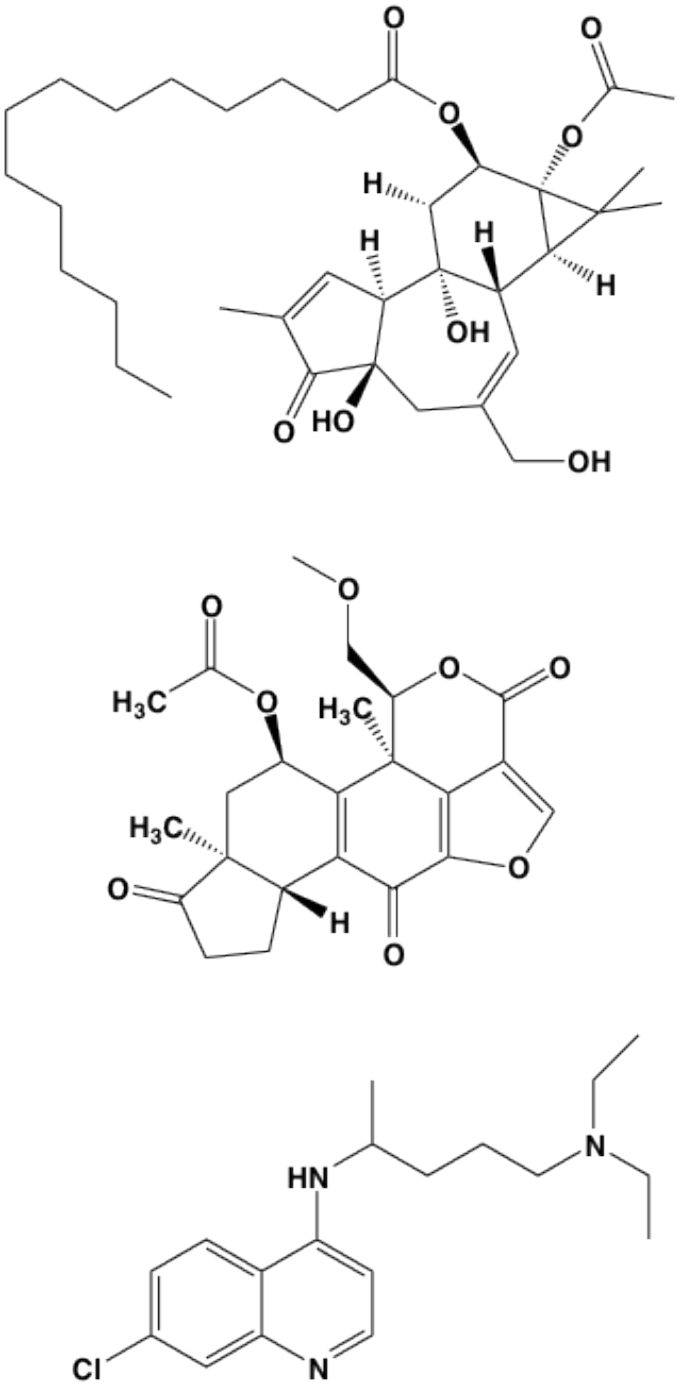

Figure 5.1 – *(top)* Phorbol 12-myristate 13-acetate, *(middle)* wortmannin, *(bottom)* chloroquine

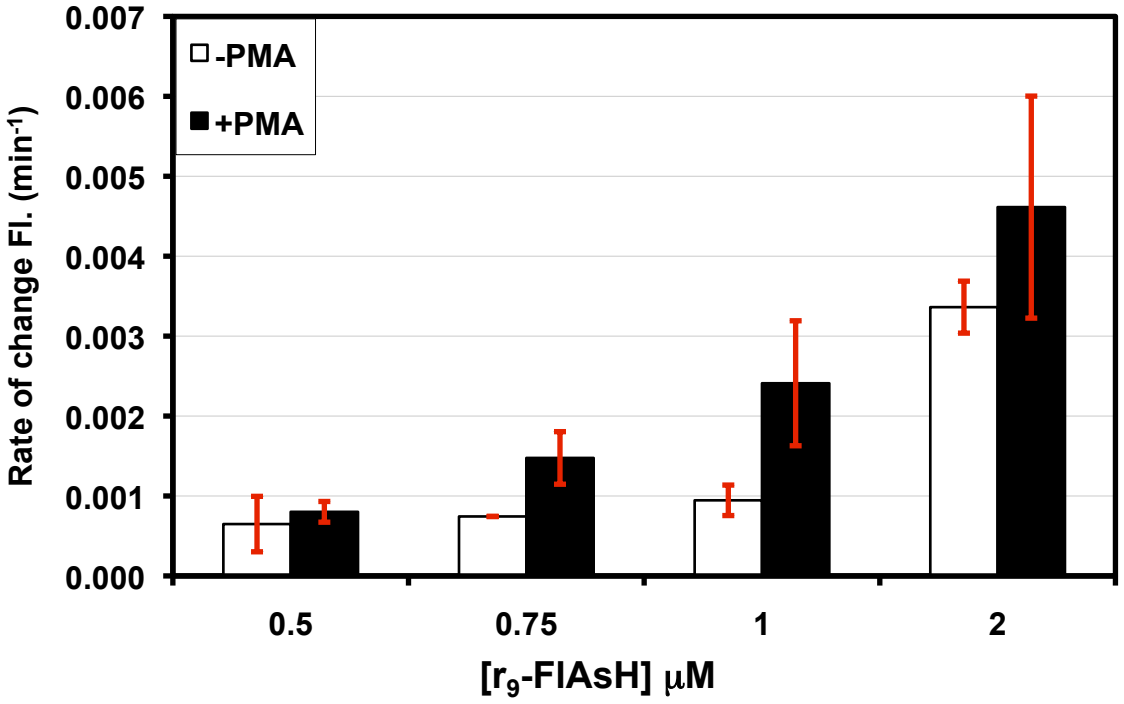

Figure 5.2 – The effect of PMA application on the delivery rate of r_9-FlAsH.

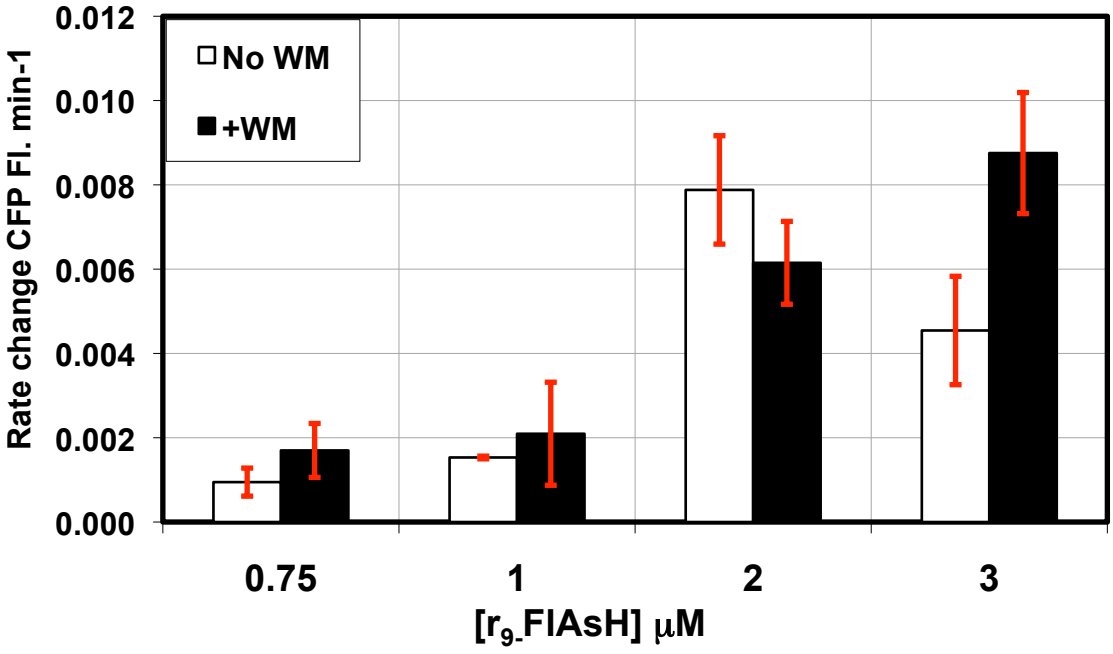

Figure 5.3 – The effect of Wortmannin (WM) application on the delivery rate of r_9-FlAsH.

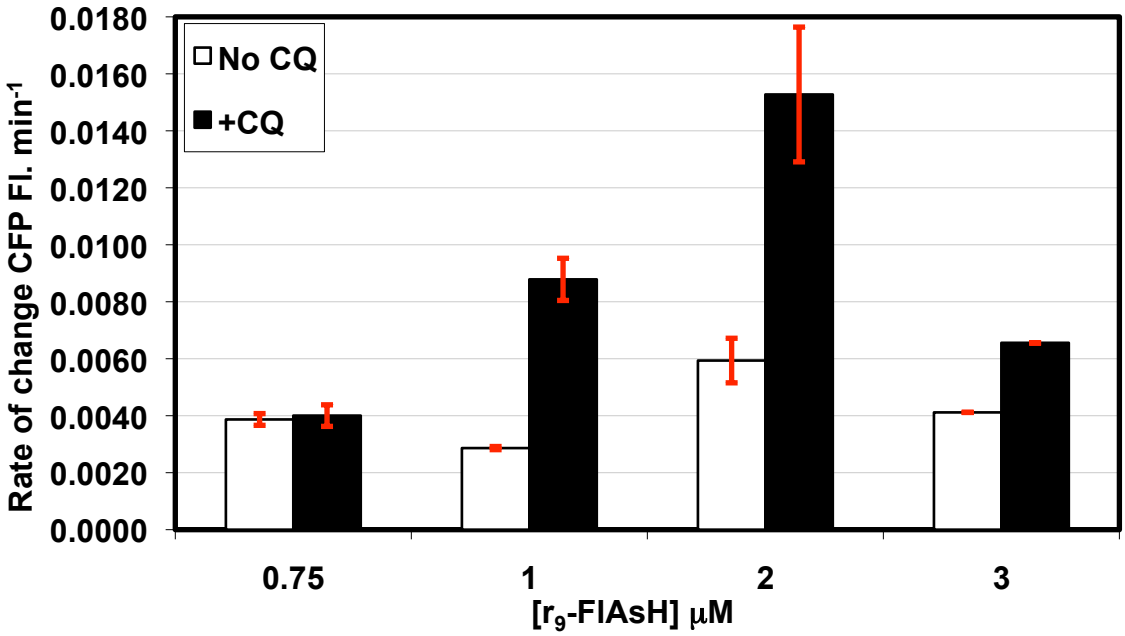

Figure 5.4 – The effect of Chloroquine (CQ) application on the delivery rate of r_9-FlAsH.

References

1. Payne, C. K., Jones, S. A., Chen, C., and Zhuang, X. (2007) Internalization and Trafficking of Cell Surface Proteoglycans and Proteoglycan-Binding Ligands, *Traffic 8*, 389–401.

2. El-Sayed, A., Futaki, S., and Harashima, H. (2009) Delivery of Macromolecules Using Arginine-Rich Cell-Penetrating Peptides: Ways to Overcome Endosomal Entrapment, *The AAPS journal 11*, 13–22.

3. Perrais, D., and Merrifield, C. (2005) Dynamics of endocytic vesicle creation, *Developmental Cell 9*, 581–592.

4. Nakase, I., Niwa, M., Takeuchi, T., Sonomura, K., Kawabata, N., Koike, Y., Takehashi, M., Tanaka, S., Ueda, K., and Simpson, J. (2004) Cellular uptake of arginine-rich peptides: roles for macropinocytosis and actin rearrangement, *Molecular Therapy 10*, 1011–1022.

5. Backer, J. (2000) Phosphoinositide 3-Kinases and the Regulation of Vesicular Trafficking, *Molecular Cell Biology Research Communications 3*, 193–204.

6. Duchardt, F., Mleczek, M. F., and Schwarz, H. (2007) A Comprehensive Model for the Cellular Uptake of Cationic Cell-penetrating Peptides, *Traffic 8*, 848–866.

7. Kalia, M., Kumari, S., Chadda, R., Hill, M. M., Parton, R. G., and Mayor, S. (2006) Arf6-independent GPI-anchored Protein-enriched Early Endosomal Compartments Fuse with Sorting Endosomes via a Rab5/Phosphatidylinositol-3'-Kinase-dependent Machinery, *Molecular Biology of the Cell, Am Soc Cell Biol 17*, 3689.

8. Fischer, R., Fotin-Mleczek, M., Hufnagel, H., and Brock, R. (2005) Break on through to the other side-biophysics and cell biology shed light on cell-penetrating peptides, *Chembiochem 6*, 2126–2142.

9. Aballay, A., Stahl, P. D., and Mayorga, L. S. (1999) Phorbol ester promotes endocytosis by activating a factor involved in endosome fusion., *Journal of Cell Science 112*, 2549–2557.

Appendix One

Gene sequence of CFP-4Cys coded as CFPPG777

CFP-PG777 pCDNA3 construct flanked by T7 promoter and SP6 Reverse sequencing promotor

```
   1  M   V   S   K   G   E   E   L   F   T   G   V   V   P   I   L   V   E   L   D
 280 ATG GTG AGC AAG GGC GAG GAG CTG TTC ACC GGG GTG GTG CCC ATC CTG GTC GAG CTG GAC

  21  G   D   V   N   G   H   R   F   S   V   S   G   E   G   E   G   D   A   T   Y
 340 GGC GAC GTA AAC GGC CAC AGG TTC AGC GTG TCC GGC GAG GGC GAG GGC GAT GCC ACC TAC

  41  G   K   L   T   L   K   F   I   C   T   T   G   K   L   P   V   P   W   P   T
 400 GGC AAG CTG ACC CTG AAG TTC ATC TGC ACC ACC GGC AAG CTG CCC GTG CCC TGG CCC ACC

  61  L   V   T   T   L   T   W   G   V   Q   C   F   S   R   Y   P   D   H   M   K
 460 CTC GTG ACC ACC CTG ACC TGG GGC GTG CAG TGC TTC AGC CGC TAC CCC GAC CAC ATG AAG

  81  Q   H   D   F   F   K   S   A   M   P   E   G   Y   V   Q   E   R   T   I   F
 520 CAG CAC GAC TTC TTC AAG TCC GCC ATG CCC GAA GGC TAC GTC CAG GAG CGT ACC ATC TTC

 101  F   K   D   D   G   N   Y   K   T   R   A   E   V   K   F   E   G   D   T   L
 580 TTC AAG GAC GAC GGC AAC TAC AAG ACC CGC GCC GAG GTG AAG TTC GAG GGC GAC ACC CTG

 121  V   N   R   I   E   L   K   G   I   D   F   K   E   D   G   N   I   L   G   H
 640 GTG AAC CGC ATC GAG CTG AAG GGC ATC GAC TTC AAG GAG GAC GGC AAC ATC CTG GGG CAC

 141  K   L   E   Y   N   Y   I   S   H   N   V   Y   I   T   A   D   K   Q   K   N
 700 AAG CTG GAG TAC AAC TAC ATC AGC CAC AAC GTC TAT ATC ACC GCC GAC AAG CAG AAG AAC

 161  G   I   K   A   H   F   K   I   R   H   N   I   E   D   G   S   V   Q   L   A
 760 GGC ATC AAG GCC CAC TTC AAG ATC CGC CAC AAC ATC GAG GAC GGC AGC GTG CAG CTC GCC

 181  D   H   Y   Q   Q   N   T   P   I   G   D   G   P   V   L   L   P   D   N   H
 820 GAC CAC TAC CAG CAG AAC ACC CCC ATC GGC GAC GGC CCC GTG CTG CTG CCC GAC AAC CAC

 201  Y   L   S   T   Q   S   A   L   S   K   D   P   N   E   K   R   D   H   M   V
 880 TAC CTG AGC ACC CAG TCC GCC CTG AGC AAA GAC CCC AAC GAG AAG CGC GAT CAC ATG GTC

 221  L   L   E   F   V   T   A   A   G   I   T   L   G   M   D   E   L   Y   K   A
 940 CTG CTG GAG TTC GTG ACC GCC GCC GGG ATC ACT CTC GGC ATG GAC GAG CTG TAC AAG GCC

 241  E   A   A   A   R   E   A   C   C   P   G   C   C   A   R   A   *
1000 GAG GCC GCC GCC AGG GAG GCC TGC TGC CCC GGC TGC TGC GCC AGG GCC TAA
```

Figure A1.1 – Gene sequence of CFP-4Cys coded as CFPPG777.

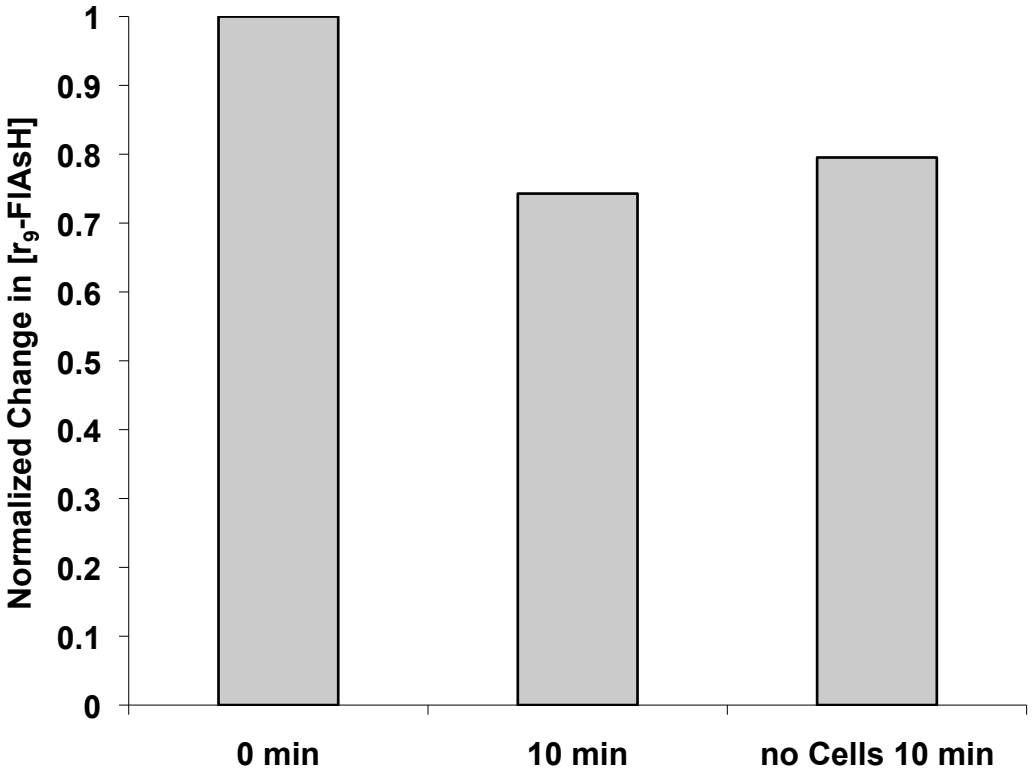

Figure A1.2 – Loss of soluble r_9-FlAsH to non-specific binding to plastic in dishes without and with cells. The adherence to cells is not significant

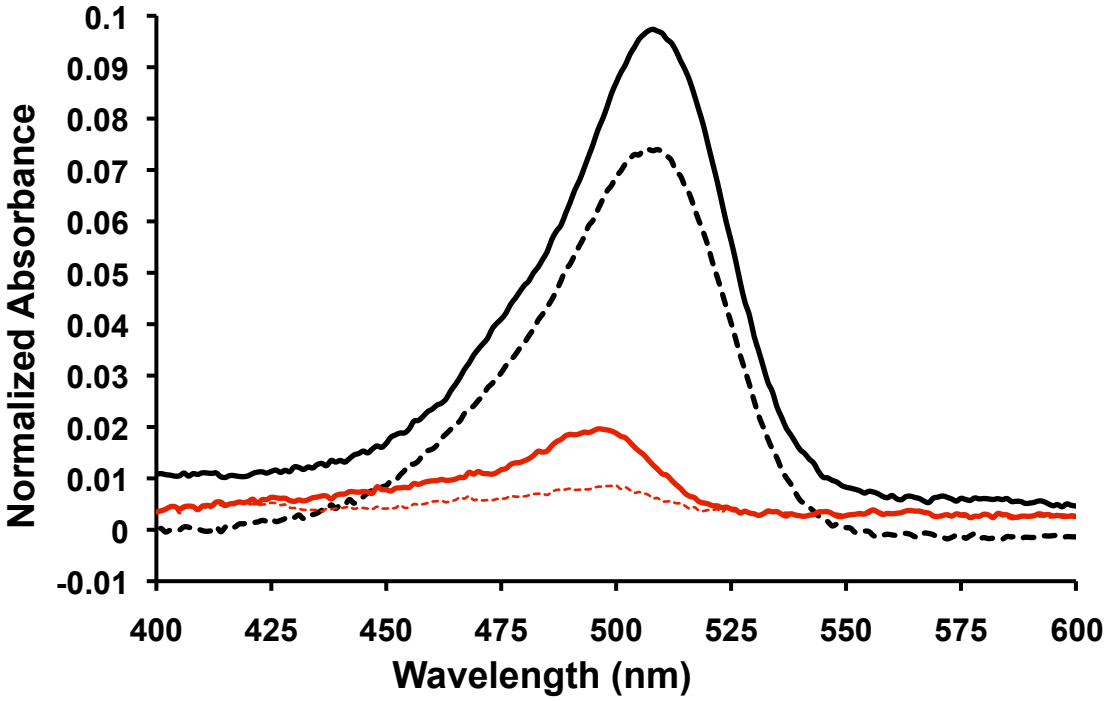

Figure A1.3 – Depletion of r_9-FlAsH in wells at 2 different concentrations. Low concentration (red line), high concentration (black line), initial time (solid), final time (60 minutes) (dashed).

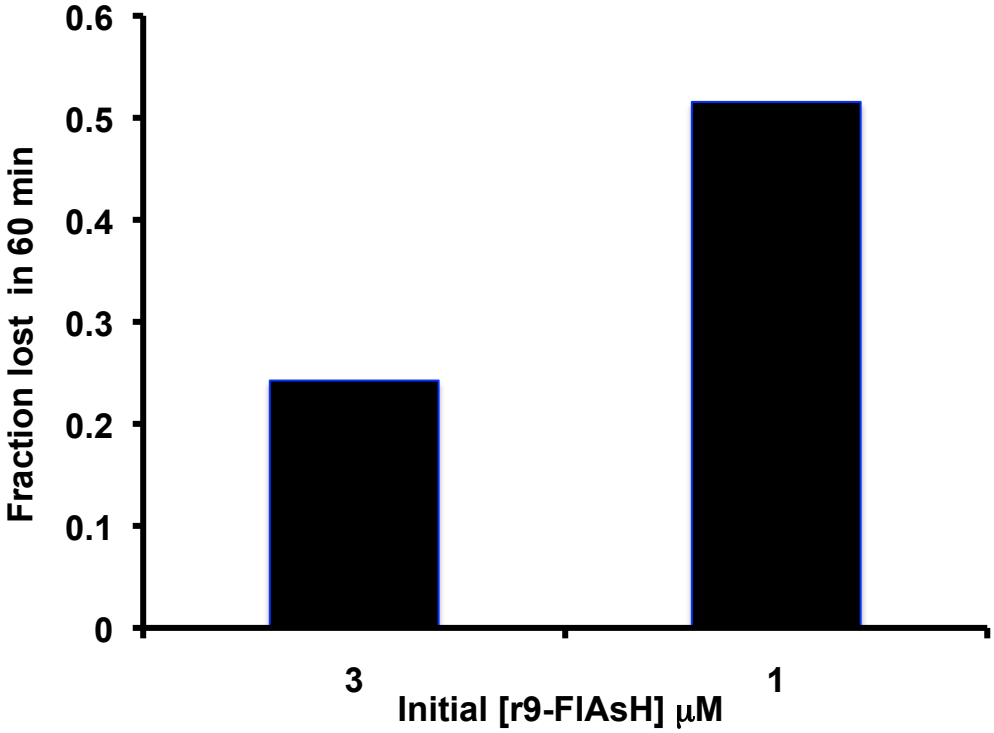

Figure A1.4 – Fraction of r_9-FlAsH that is depleted from solution in wells (3 μM and 1 μM).

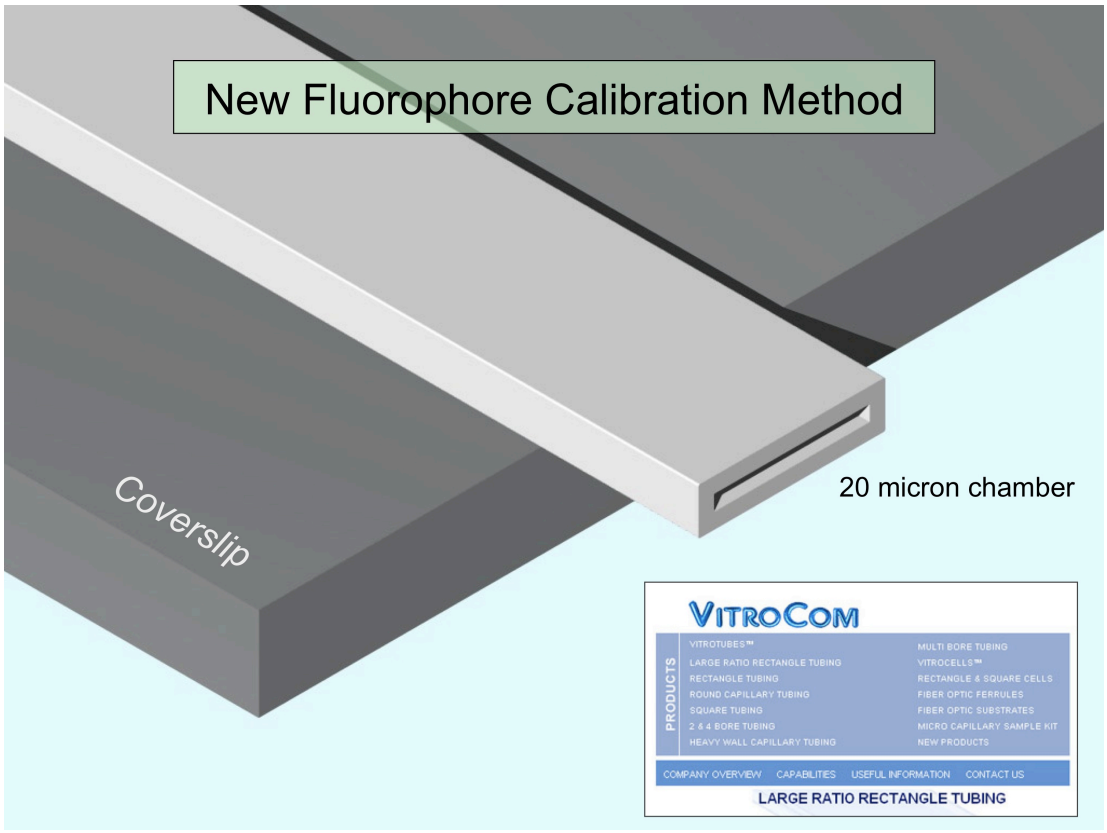

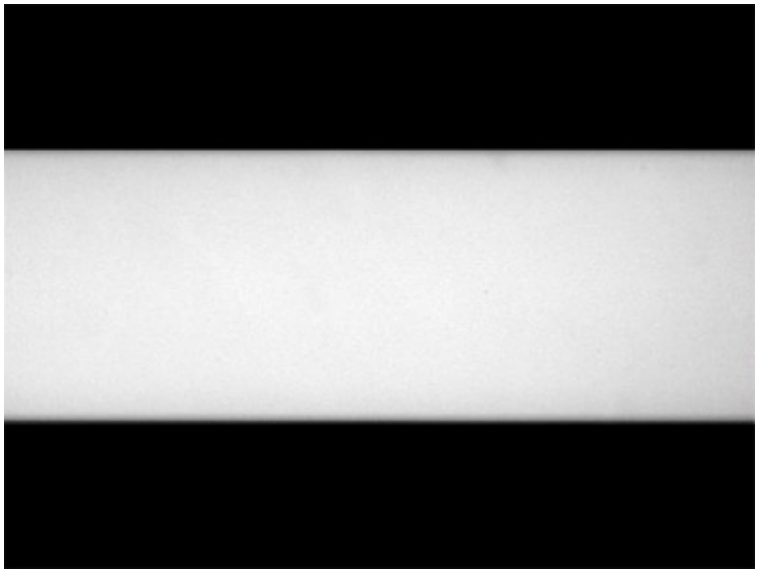

Figure A1.5 – *(above)* CAD rendering of micro-cuvettes used for calibration of fluorescent molecules. *(below)* Fluorescent image of micro-cuvette filled with fluorescent liquid as seen in epifluorescence image.

InputCellObject.java

```
// File:  InputCellObjects.java

import java.io.*;

public class InputCellObject {

    public static void main(String args[]) {
        //... Get two file names from user.

      /****************

       System.out.println("Enter a filepath to input from");
      //  Scanner in = new Scanner(System.in); //reads the input from
the CONSOLE from User

      *///////////////

        //... Create File objects.2

        for (int i = 0; i < args.length; i++) {
            File inFile  = new File(args[i]);  // File to read from is
first read-in string
            String [] outputFile = args[i].split(".txt");

            String outputFileName = outputFile[0]+"_out.txt";
            System.out.println("Output: " + outputFileName);
        //... Create output File object
            File outFile = new File(outputFileName);  // File to write
to is the second read-in string

        //... Enclose in try..catch because of possible io exceptions.
            try {
              getData(inFile, outFile);

            } catch (IOException e) {
              System.err.println(e);
                System.exit(1);
            }
        }
    }
```

Figure A1.6 – Main method of program to process the data written in JAVA programming language. The main method runs the main portion of the program from a command prompt window. This portion of the code creates data structures to organize the data from each cell and position (continued on the next four pages).

```
      //============================================================
getData(fromFile, toFile)
    // Uses Scanner for file input.
    public static void getData(File fromFile, File toFile) throws
IOException {
        BufferedReader breader = new BufferedReader(new FileReader
(fromFile));
        BufferedWriter writer = new BufferedWriter(new FileWriter
(toFile));


        StringTokenizer st;
        Cell[] CellArray = new Cell[10];
        Cell c;

        String line = null;
        String token = null;
        String dataLine;

        int i = 0;
        int cellIndex = 0;

        /* READ through first few lines of file and copy to File
indicated to write to */
        line = breader.readLine();
        for (i = 0; i<3; i++)   {
            writer.write(line);
            writer.newLine();
            line = breader.readLine();
        }

        line = breader.readLine(); //Reading Object # line

         //... Loop as long as there are input lines.
        while (line != null)    {

                st = new StringTokenizer(line);

                if (line.contains("Object"))    //once you find "Object"
make the cell Object
```

Figure A1.6 – Main method of program to process the data written in JAVA programming language. (Continued)

```
                    st.nextToken();//skip "Object"

                /* making new Cell Object */
                Integer CellIndex = new Integer(st.nextToken());
                c = new Cell(CellIndex.intValue());

                /* Placing Cell Objects into CellArray */

                /* if (cellIndex > 9)   {
                    CellArrayCopy =
                } */// if there are more than 10 objects in the Array it
needs to be expanded.

                CellArray[cellIndex] = c;

                /* From this point on you are reading lines of data into
BufferedReader */
                line = breader.readLine();// skipping the headings

                line = breader.readLine();// input first line of data
from BufferedReader for data file

                int dataIndex = 0;

                while (line != null && !line.contains("Object"))    {
                    StringTokenizer stokenizer = new StringTokenizer
(line);

                    /* The first token is skipped and the next token is
the time elapsed*/
                    stokenizer.nextToken();//skipping the Timepoint
index

                    Integer Time = new Integer(stokenizer.nextToken());
                    int time = Time.intValue();
                    c.setTimePoint(dataIndex, time);

                    /* The next token is the Area in sq. microns */
                    Double Area = new Double(stokenizer.nextToken());
                    double area = Area.doubleValue();
                    c.setArea(dataIndex, area);
```

Figure A1.6 – Main method of program to process the data written in JAVA programming language. (Continued)

```
                    /* The next 4 tokens are skipped b/c they are the
Mean Intensity Values*/
                    for(i = 0; i<4; i++)    {
                        stokenizer.nextToken();
                    }

                    Double SumCFP = new Double(stokenizer.nextToken());
                    double scfp = SumCFP.doubleValue();
                    c.setSumCFP(dataIndex, scfp);

                    //remaining tokens are skipped because I don't
currently use them in my Analysis
                    line = breader.readLine();
                    dataIndex++;

                }// end small While loop when line contains "Object"

                cellIndex++; // increment the index for input of NEXT
cell; note that this is 1 more than # of cells

        }// end large While loop when line == null
        System.out.println("Input Data: COMPLETE");
        correctCellCounts(CellArray, cellIndex, writer);
            //... Close reader and writer.

            // Write system dependent end of line.

        breader.close();  // Close to unlock.
        writer.close();  // Close to unlock and flush to disk.
    }

    public static void correctCellCounts(Cell [] cells, int count,
BufferedWriter bw)  {
        /* correction calculator for cells */

        int bckgdIndex = seekBackground(cells, count);  // calling the
seekBackground Method to
                                                        // identify the
Background Object/Cell
```

Figure A1.6 – Main method of program to process the data written in JAVA programming language. (Continued)

```
        Cell bckgdcell = cells[bckgdIndex]; //identifying the background
Cell
        int capacity = bckgdcell.getNumpoints();  //getting the capacity
of the background Cell array; the number of timepoints
        double bckgdArea = bckgdcell.getArea(0).doubleValue();  //
getting the actual Area of the background region


        for(int i=0; i < count; i++)    {
            if (i == bckgdIndex)    {

                Cell c = cells[i];
                double originalArea; //= c.getArea(i).doubleValue();
                double correctedAreaFactor;

                double originalValue;
                //System.out.println(originalValue);
                double backgroundValue;
                double correctionFactor;
                double correctedValue;

                /*The following code is going to iterate through the
areas, determine a correction factor and
                  subtract the corrected background from the CFP counts
and determing the corrected SumCFP.*/
                for (int index = 0; index < capacity; index++)  {
                    originalArea = c.getArea(index).doubleValue
(); /////////////// added in August 04, 2009
                    correctedAreaFactor = originalArea/bckgdArea;
                    originalValue = c.getSumCFP(index).doubleValue();

                    backgroundValue = bckgdcell.getSumCFP
(index).doubleValue();

                    correctionFactor = backgroundValue *
correctedAreaFactor;

                    correctedValue = originalValue - correctionFactor;
                    c.setCorrectedSumCFP(index, correctedValue);
                    //System.out.println("Corrected");
                }
```

Figure A1.6 – Main method of program to process the data written in JAVA programming language. (Continued)

Cell.java

```
import java.io.*;

// File Name: Cell.java
// Description:  Creates Cell Class to hold attributes of Cell
//                  including Time point, elapsed Time (ms), etc.

public class Cell   {

    public ArrayList<Double> TimePoint;
    public ArrayList<Double> Area; /*MeanCFP<Double>, MeanFlAsH,
MeanFRET, MeanPI,*/
    public ArrayList<Double> SumCFP;/*, SumFlAsH, SumFRET, SumPI,*/
    public ArrayList<Double> CorrSumCFP;
    private int objectNum, numpoints;
    private double elapMin;
    private boolean isBackground = false;

    public Cell (int objectIndex)   {
        objectNum = objectIndex + 1;
        TimePoint = new ArrayList();
        Area = new ArrayList();
        SumCFP = new ArrayList();
        CorrSumCFP = new ArrayList();
        int numpoints = 0;

        //ArrayList MeanCFP = new ArrayList();
        //ArrayList MeanFlAsH = new ArrayList();
        //ArrayList MeanFRET = new ArrayList();
        //ArrayList MeanPI = new ArrayList();
        //ArrayList SumCFP = new ArrayList();
        //ArrayList SumFlAsH = new ArrayList();
        //ArrayList SumFRET = new ArrayList();
        //ArrayList SumPI = new ArrayList();

    }

    public int getObjectNum()   {
        return objectNum;
    }

    public void setTimePoint(int index, int t)  {
```

Figure A1. 7 – Cell class file of program to process the fluorescence counts data collected from each cell; written in JAVA programming language. Class that creates a cell object holding all data values of each cell. (continued on the next four pages).

```
    elapMin = (double)t/(1000*60);

    Double D = new Double(elapMin);
    TimePoint.add(index, D);
    incrementNumpoints();
}

public Double getTimePoint (int index)  {
    return (Double)TimePoint.get(index);
}

public void setArea(int index, double area) {
    Area.add(index, new Double(area));
}

public Double getArea(int index)    {
    return (Double)Area.get(index);
}

public void setSumCFP(int index, double scfp)   {
    Double d = new Double(scfp);

    SumCFP.add(index, d);
}

public Double getSumCFP(int index)  {
    Double d = new Double(SumCFP.get(index));
    return d;
}

public Double getCorrectedSumCFP (int index)    {
    Double d = new Double(CorrSumCFP.get(index));
    return d;
}

public void setCorrectedSumCFP(int index, double correctedSum)  {
    Double CorrectedSum = new Double(correctedSum);
    CorrSumCFP.add(index, CorrectedSum);
}

public void setBackground(boolean flag) {
```

Figure A1. 7 – Cell class file of program to process the fluorescence counts data collected from each cell. (Continued)

Cell.java

```
        isBackground = flag;
    }

    public void incrementNumpoints()    {
        numpoints++;
    }

    public int getNumpoints()   {
        return numpoints;
    }

    public void writeOut(BufferedWriter bw) {
        int i = 0;
        try {
            for (i = 0; i < getNumpoints(); i++)    {
                if(i == 0)  {
                    if (isBackground)
                        bw.write("BACKGROUND");
                    else
                        bw.write("Object " + getObjectNum());// Object
number

                    bw.newLine();
                    bw.write("Elapsed Time (min),Area (sq. microns),CFP
Counts, Corr.CFP Counts"); // Headings for data
                    bw.newLine();
                }
                bw.write(getTimePoint(i).toString() + ",");
                bw.write(getArea(i).toString() + ",");
                bw.write(getSumCFP(i).toString() + ",");
                bw.write(getCorrectedSumCFP(i).toString());
                bw.newLine();
            }

        }
        catch (IOException e) {
          System.err.println(e);
          System.exit(1);
        }
    }
```

Figure A1. 7 – Cell class file of program to process the fluorescence counts data collected from each cell. (Continued)

```
/*public void setMeanCFP(int index, double mcfp)    {
        MeanCFP.add(index, new Double(mcfp));
    }

    public Double getMeanCFP(int index) {
        return (Double)MeanCFP.get(index);
    }

    public void setMeanFlAsH(int index, double mflash)  {
        MeanFlAsH.add(index, new Double(mflash));
    }

    public Double getMeanFlAsH(int index)   {
        return (Double)MeanFlAsH.get(index);
    }

    public void setMeanFRET(int index, double mfret)    {
        MeanFRET.add(index, new Double(mfret));
    }

    public Double getMeanFRET(int index)    {
        return (Double)MeanFRET.get(index);
    }

    public void setMeanPI(int index, double mpi)    {
        MeanPI.add(index, new Double(mpi));
    }

    public Double getMeanPI(int index)  {
        return (Double)MeanPI.get(index);
}*/
/*public void setSumFlAsH(int index, double sflash) {
        SumFlAsH.add(index, new Double(sflash));
    }

    public Double getSumFlAsH(int index)    {
        return (Double)SumFlAsH.get(index);
    }

    public void setSumFRET(int index, double sfret) {
        SumFRET.add(index, new Double(sfret));
```

Figure A1. 7 – Cell class file of program to process the fluorescence counts data collected from each cell. (Continued)

```
        }

        public Double getSumFRET(int index) {
            return (Double)SumFRET.get(index);
        }

        public void setSumPI(int index, double spi) {
            SumPI.add(index, new Double(spi));
        }

        public Double getSumPI(int index)   {
            return (Double)SumPI.get(index);
    }*/
}
```

Figure A1. 7 – Cell class file of program to process the fluorescence counts data collected from each cell. (Continued)

Preparation of r_9-FlAsH-O.

15 nmol r_9-FlAsH$(EDT)_2$ was mixed with 39 nmole Mercuric acetate ($HgAc_2$) in THF. Reaction results in a cloudy mixture. Mixture was centrifuged and supernatant was checked for full reaction on UV/Vis (525 nm). Reaction appeared complete. Supernatent was lyophilized and resulted in a shiny gold residue.